Surfaces and Interfaces 96 (2026) 109958

Contents lists available at ScienceDirect

Surfaces and Interfaces

journal homepage: www.sciencedirect.com/journal/surfaces-and-interfaces

# Novel asymmetric liquid crystalline ZnPc thin films for optical surface plasmon resonance sensor applications to dichloromethane vapor: Design, synthesis, preparation, characterization, and the influence of the substituent group on the sensor response

Zeynep Özer [a], Gizem Gümüşgöz Çelik [a], İnci Çapan [b], Rifat Çapan [b,*], Ayşe Gül Gürek [a,*]

[a] Gebze Technical University, Science Faculty, Chemistry Department, 41400, Gebze, Kocaeli Turkey
[b] Balikesir University, Science&literature Faculty, Physics Department, 10145, Balikesir, Turkey

ARTICLE INFO

*Keywords:*
Zinc(II) phthalocyanine
Asymmetric phthalocyanine
Liquid-crystalline
Elovich model
Surface plasmon resonance
Dichloromethane vapor sensor

ABSTRACT

This study aims to synthesize two newly designed, soluble asymmetrically substituted Zn(II) phthalocyanines (ZnPc1-$A_3B$ and ZnPc2-$AB_3$) exhibiting liquid crystalline behavior, aimed at improving their chemiresistive sensing performance towards dichloromethane vapor. They were characterized using Nuclear Magnetic Resonance, Ultraviolet-visible, and Fourier Transform Infrared spectroscopies, together with mass spectrometry. Polarizing Optical Microscopy, X-ray Diffraction, and Differential Scanning Calorimetry techniques were employed to determine phase transition temperatures. The formation of a columnar hexagonal ($Col_h$) mesophase for ZnPc1-$A_3B$ and a rectangular columnar ($Col_r$) mesophase for ZnPc2-$AB_3$ was confirmed over a wide temperature range by complementary methods. The observed phase transition temperatures were found to be strongly dependent on the nature of the substituents.

Spin coating and Surface Plasmon Resonance techniques were employed to fabricate thin film sensors and to investigate the influence of phthalocyanine molecular architecture and the controlled incorporation of polyoxyethylene and alkylthio substituents on sensor behavior. For the detection of dichloromethane vapor, the ZnPc1-$A_3B$ thin film sensor produced the highest sensitivity, the lowest limit of detection, and limit of quantification values compared with the ZnPc2-$AB_3$ thin film sensor. It is shown that the polyoxoethylene side chains having oxygen atoms play an important role in enhancing sensor performance before and after heating processes. The Elovich model was employed to determine the adsorption rate constants. This study improved gas sensor performance using Zn(II) phthalocyanine derivatives, optimizing the number of the substituents on the sensor response, and showed that the ZnPc1-$A_3B$ thin film sensor is a good candidate for an optical-based sensor in the field of environmental monitoring or dichloromethane vapor detection.

## 1. Introduction

Phthalocyanines (Pcs) are highly robust, predominantly planar macrocyclic compounds whose physicochemical characteristics can be finely tuned through rational molecular design [1]. In metallo phthalocyanines (MPcs), key properties are governed by the nature of the coordinated metal ion, the substitution pattern on the macrocycle, the presence of axial ligands when relevant, and the surrounding chemical environment [2,3]. Owing to this structural versatility, Pcs have emerged as functional materials in a broad range of fields, including organic electronics [4], photodynamic therapy [5–7] chemical sensing [8,9] catalysis [10], and photovoltaic technologies [11–13]. Coordination with metal centers such as zinc, copper, or cobalt enhances charge transport and electron-transfer processes, thereby expanding their applicability [14,15]. The position and intensity of the characteristic Q-band absorption are particularly sensitive to substituent effects on the Pc framework, with electron-donating or electron-withdrawing groups inducing notable spectral shifts [16]. The introduction of electron-donating alkoxy groups, polyoxyethylene (POE) chains, and alkylthio (–SR) substituents enhances molecular solubility while

* Corresponding authors.
*E-mail addresses:* rcapan@balikesir.edu.tr (R. Çapan), gurek@gtu.edu.tr (A.G. Gürek).

https://doi.org/10.1016/j.surfin.2026.109958
Received 30 March 2026; Received in revised form 10 June 2026; Accepted 24 June 2026
Available online 27 June 2026

simultaneously reducing strong intermolecular π–π stacking. This attenuation of aggregation effects is crucial, as excessive self-association commonly compromises the optoelectronic and photophysical properties of phthalocyanine-based materials [17]. Moreover, the inherent planarity of Pcs facilitates strong interfacial interactions and efficient adsorption onto diverse substrates. Their extended π-conjugated systems render them highly responsive to local electronic perturbations, enabling enhanced sensitivity and selectivity towards a variety of analytes, including volatile organic compounds, environmental contaminants, and hazardous gases such as ammonia and carbon monoxide [18,19]. Furthermore, the incorporation of these substituent groups into the phthalocyanine core induces liquid crystalline behavior, favoring the formation of well-defined columnar mesophases that are characteristic of discotic phthalocyanine systems.

Discotic metal phthalocyanines bearing flexible alkyl or POE chains frequently exhibit liquid crystalline behavior and have emerged as promising functional materials for a wide range of electronic applications, particularly in chemical sensing devices [20,21]. Their ability to self-assemble into well-organized thin films with tunable molecular orientation enables precise control over charge-transport properties. In such systems, π–π interactions between adjacent phthalocyanine cores lead to the formation of columnar architectures, where charge carriers preferentially migrate along the stacking direction, resulting in pronounced anisotropic electrical conductivity.

Despite extensive investigations into the sensing behavior of phthalocyanine-based materials, the vast majority of reported studies have been confined to symmetrically substituted derivatives [20,22,23]. Remarkably, gas-sensing studies on asymmetrically substituted phthalocyanines that also display liquid crystalline mesomorphism are exceedingly scarce. This pronounced lack of research highlights an important knowledge gap, which the present work seeks to address by systematically evaluating the gas-sensing performance of liquid crystalline asymmetric phthalocyanine derivatives [24–27]. Although several studies in the literature have investigated the sensing properties of asymmetric phthalocyanines, these studies have mainly focused on their sensing responses toward various gases such as ammonia [28] and $NO_2$, as well as pesticides [29] and alcohols [30]. In particular, studies on liquid crystalline asymmetric phthalocyanine derivatives containing polyoxyethylene chains are quite limited, and these compounds have generally been used in combination with single-walled carbon nanotubes (SWNTs) for ammonia gas sensing applications [31,32].

In thin film characterization and volatile organic vapor (VOC) sensor applications, the optical surface plasmon resonance (SPR) technique is widely employed using thin film sensors to monitor the amount of VOC due to its high resolution, ease of use, rapid detection, and real-time measurement capabilities [33,34]. Dichloromethane (DCM) is a volatile, colorless liquid with an odor. DCM is a powerful industrial solvent across pharmaceutical, laboratory, and manufacturing sectors and is widely used in many industrial settings, including paint stripping solutions and the manufacture of pharmaceuticals. In case of DCM exposure, it irritates the skin and eyes by preventing evaporation, and it causes chemical burns in the long term. Its main toxic damages can be given as reversible central nervous system depression (neurophysiological and neurobehavioral disturbances) and carboxyhemoglobin formation, extending up to renal, hepatic, cardiovascular, and hematological effects [35,36].

In the literature, there are very limited studies on the detection of DCM vapor using liquid crystalline Zn(II) phthalocyanine derivatives [37]. However, different Zn(II) phthalocyanine derivatives were used to study VOC sensor applications using DCM [38,39], ammonia [40,41], toluene, acetone, chloroform, isopropanol, ethanol, methanol, and carbon tetrachloride [42–45] vapors. In addition, to the best of our knowledge, there is no report in the literature investigating the sensing properties of liquid crystalline asymmetric phthalocyanine derivatives containing polyoxyethylene chains toward chlorinated volatile organic compounds using the SPR technique. Moreover, in the limited number of SPR-based sensing studies employing phthalocyanine derivatives, symmetric phthalocyanines have generally been preferred as sensing materials [34,39,42,46,47]. All these findings clearly demonstrate that this present study contributes to filling an important gap in the literature. The obtained results demonstrate the significant potential of these functional liquid crystalline phthalocyanines for advanced optical sensing applications.

Our previous study focused on the heating effect over the detection of chlorinated hydrocarbon vapors using a symmetrical liquid-crystalline octakis(hexylthio)zinc(II) phthalocyanine (ZnPc2-$B_4$) spun thin film sensor, aiming to identify the interaction patterns between the reactive sites of the thin film sensor and the vapor molecules [37]. The results showed that Zn interacts with the nucleophilic carbon atom of the vapor, thereby interacting with the π-electrons of the C=C double bond. In addition, C···Cl, Zn···Cl, and N···H interactions occurred between the symmetrical thin film sensor and vapor molecules. Following the promising sensor response of the thin film sensor, we decided to further investigate the same core of ZnPc2 with different side molecular groups.

The novelty of this article can be defined as follows: it involves the synthesis of completely new materials and the investigation of their interactions with DCM vapor, which is made possible by differences in their molecular structures. A rational molecular design (Fig. 1) based on asymmetric $AB_3$-type phthalocyanines (ZnPc1-$A_3B$ and ZnPc2-$AB_3$) incorporating controlled numbers of weak and strong electron-donating substituents as 4-(2-(2-ethoxyethoxy)ethoxy)phthalonitrile (PN1) and 4,5-bis(hexylthio)phthalonitrile (PN2) is introduced. The reduced symmetry of the $AB_3$ architecture suppresses aggregation and improves film homogeneity, which are essential for reproducible chemiresistive responses. By correlating substituent donor strength with resistance changes toward dichloromethane vapor, this work provides insight into structure–property–response relationships in phthalocyanine-based gas sensors. We demonstrate the contributions of the molecular structure of the Pc and the number of polyoxyethylene and alkylthio substituents to the Pc to sensitivity and selectivity in VOC detection. In addition, the articles' originality can be further defined by investigating the behavior of the dichloromethane vapor sensor in response, both before and after heating.

In this study, we report the synthesis of two newly designed, soluble, asymmetrically substituted Zn(II) phthalocyanines (Fig. 1) that exhibit liquid-crystalline behavior, with the aim of improving their chemiresistive sensing performance toward DCM vapor. These phthalocyanine derivatives were designed to provide accessible coordination environments that promote efficient analyte–sensor interactions. Polyoxyethylene and alkylthio substituents were intentionally selected due to their distinctly different electron-donating strengths, enabling systematic modulation of the electronic structure of the phthalocyanine core. While polyoxyethylene chains primarily influence solubility, film morphology, and interfacial interactions, alkylthio groups offer stronger electronic coupling with the π-conjugated macrocycle. The thin-film sensors were prepared using the spin-coating fabrication method. Optical properties and sensor behavior were studied using a SPR measurement system. A comprehensive study was conducted on the design, synthesis, and functional characterization of two novel asymmetric zinc (II) phthalocyanines (ZnPc1-$A_3B$ and ZnPc2-$AB_3$) for the detection of dichloromethane vapor by optical surface plasmon resonance. It was systematically investigated how the controlled incorporation of polyoxyethylene and alkylthiosubstituents, coupled with molecular asymmetry, influences liquid crystal mesophase formation, thin-film morphology, and analyte-sensor interactions. The Elovich model for adsorption dynamics was applied to SPR experimental data and the adsorption rate constants of ZnPc1-$A_3B$ and ZnPc2-$AB_3$ thin films before and after heating process were calculated with correlation coefficients of $>0.95$. This research combines synthetic chemistry, photophysical characterization, mesophase analysis, and detection measurements, which may be of interest to the fields of physical chemistry, materials

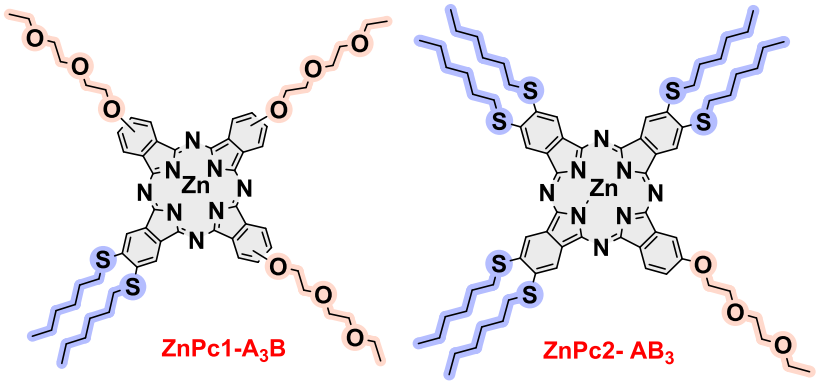


**Fig. 1.** Molecular structure of asymmetric phthalocyanine derivatives (ZnPc1-$A_3B$, ZnPc2-$AB_3$).

science, and sensor technology.

## 2. Experimental details

Details of the equipment and materials used, along with the photophysical and photochemical measurements, and the synthesis of 4-(2-(2-ethoxyethoxy)ethoxy)phthalonitrile (PN1) and spectroscopic data related to the characterization of the compounds, are provided in the Supporting Information Section S1-S4.

### 2.1. Synthesis of ZnPc1-$A_3B$

500 mg (1.91 mmol, 10 eqv) of PN1 and 68 mg (0.191 mmol, 1 eqv) of PN2 were transferred into a reaction flask under an $Ar_{(g)}$. Then, 2 mL of dry DMF and 200 μL of 1,8-diazabicyclo[5.4.0]undec-7-ene (DBU) were added. Subsequently, 87 mg (476.54 μmol, 2.5 eqv) of dry zinc acetate ($Zn(OAc)_2$) were introduced to the mixture (Scheme 2). The reaction mixture was then stirred at reflux temperature overnight under a cooling condenser. After completion of the reaction, the mixture was transferred into cold water (100 mL) and extracted with DCM. The resulting crude material was purified by silica gel column chromatography employing DCM:EtOH solvent mixtures of 50:1 and 20:1, enabling the separation of symmetric and asymmetric products. The asymmetric and symmetric Pc derivatives were further purified with preparative TLC plates using a mixture of *n*-hexane-dioxane (2:1). As a result, a green colored viscous ZnPc1-$A_3B$ (36 mg, 14%) and ZnPc1-A4 (125 mg, 26%) were obtained. $C_{62}H_{76}N_8O_9S_2Zn$, Mw: 1206,84 g/mol. FT-IR [(ATR) $\nu_{max}/cm^{-1}$]: 2995–2882 ($CH_2$), 1607, 1488, 1452, 1386, 1337, 1278, 1235,1092, 1052, 955, 854, 827, 750. MALDI-TOF-MS (DHB): *m/z* Calcd: 1206.84 g/mol, Found: 1206.140 $[M+H]^+$.$^1$H NMR (500 MHz, THF-$d_8$): $\delta$ 8.89, 8.81, 8.78, 8.46, 8.34, 8.21, 8.10, 7.66, 7.61, 7.53, 7.34, 4.66, 4.20, 3.92, 3.76, 3.58, 3.47, 2.48, 2.06, 1.73, 1.57, 1.27, 1.05 ppm. $^{13}$C NMR (125 MHz, THF-$d_8$,): $\delta$ 161.92, 161.82, 161.73, 153.07, 152.72, 141.21, 140.77, 139.75, 132.41, 124.20, 121.72, 121.22, 118.75, 118.24, 106.98, 106.73, 106.39, 72.20, 71.36, 71.20, 71.15, 69.37, 68.10, 67.57, 35.10, 34.93, 34.60, 34.42, 32.84, 32.83, 32.64, 30.81, 30.19, 30.11, 29.34, 25.49, 24.07, 23.87, 23.84, 23.58, 16.01, 14.75, 14.61 ppm (Figures. S5-S8). Elemental analysis (%) calcd C, 61.71; H, 6.35; N, 9.29; S, 5.31, found C, 61.51; H, 6.46; N, 9.11; S, 5.27.

### 2.2. Synthesis of ZnPc2-$AB_3$

500 mg (1.39 mmol,) of PN2 and 36 mg (0.139 mmol,) of PN1 were transferred to a suitable flask under an $Ar_{(g)}$ atmosphere, followed by degassing. Then, 2 mL of dry DMF and 200 μL of DBU were added. Subsequently, 64 mg (346.67 μmol) of $Zn(OAc)_2$ were added to the mixture (Scheme 2). The reaction mixture was then stirred at reflux temperature overnight under a cooling condenser. After the reaction was terminated by precipitation in EtOH. The crude product was initially purified by DCM:EtOH (50:1) followed by (20:1) on silica gel column chromatography to separate symmetric and asymmetric structures. The asymmetric and symmetric Pc derivatives were further purified on preparative TLC plates using a mixture of DCM: EtOH (50:1). As a result, a green colored viscous ZnPc2-$AB_3$ (30 mg,16%) and ZnPc2-$B_4$ (120 mg, 31%) were obtained. $C_{74}H_{100}N_8O_3S_6Zn$, Mw: 1407.41 g/mol. FT-IR [(ATR) $\nu_{max}/cm^{-1}$]: 2955–2855 ($CH_2$), 1594, 1485, 1457, 1406, 1373, 1338, 1248, 1102, 1068, 944, 854, 827, 742. MALDI-TOF-MS (DHB): *m/z* Calcd: 1407.41 g/mol, Found: 1407.047 $[M^+H]^+$. $^1$H NMR (500 MHz, $CDCl_3$,): $\delta$ 8.25, 8.07, 8.02, 7.97, 7.72, 7.52, 7.41, 7.31, 7.24, 7.13, 4.11, 3.80, 3.56, 3.46, 3.14, 2.96, 2.71, 1.83, 1.74, 1.53, 1.33, 1.23, 1.13, 0.92, 0.84, 0.82, ppm.$^{13}$C NMR (125 MHz, $CDCl_3$,): $\delta$ 161.02, 152.00, 138.19, 137.37, 134.83, 120.07, 117.14, 77.41, 77.16, 76.91, 70.87, 69.93, 69.87, 67.98, 67.58, 66.76, 33.85, 33.63, 33.40, 32.74, 31.87, 31.78, 29.85, 29.24, 29.19, 29.13, 28.84, 28.61, 28.52, 25.32, 22.89, 22.84, 22.80, 22.58, 15.25, 14.35, 14.32 ppm (Figures S9-S12). Elemental analysis (%) calcd C, 63.15; H, 7.16; N, 7.96; S, 13.67, found C, 63.26; H, 7.27; N, 7.86, S, 13.44.

### 2.3. The thin film sensor fabrication and SPR measurements

The spin coating method was preferred to use for the fabrication of organic thin films onto a gold-coated glass substrate, which is suitable in the field of gas sensor applications. The main working principle of the spin coating technique can be defined as centrifugal dispersion of an applied solution onto a solid substrate, which is employed to rotate about the horizontal axis at a predetermined rotation speed. The centrifugal force effect provides the formation of a uniform thin film on the solid substrate. The accurate control of its acceleration and deceleration can be achieved. SPR spectrometer was employed to estimate the thickness and the optical parameters of the thin film sensors, as well as to record the real-time vapor sensing data via the reflected light intensity value. The number of replicates used in each experiment was three. Details of the spin coating system, vapor concentration values (Table S1), and SPR measurements were provided in the Supporting Information Section S3.

### 2.4. The Elovich model fitting theory

The Elovich model was chosen to elucidate the adsorption dynamics. This model is widely employed to analyze the adsorption behavior of organic thin films during the interaction between a thin film surface and a selected adsorbent. In this study, SPR real-time kinetic measurement data obtained for ZnPc1-$A_3B$ and ZnPc2-$AB_3$ thin film sensors were used to determine the adsorption capacity $(q_t)$, Elovich parameters, and correlation coefficient $(R^2)$. $R^2$ indicates the conformity between SPR experimental data and the Elovich model parameters.

For the SPR time dependent kinetic measurement data during the adsorption interaction between thin film and vapor molecules, $q_t$ is

described for the first time as [48]:

$$q_t = \left[\frac{(I_i - I_e)V}{A}\right] \quad (1)$$

where $I_i$ is the initial reflected light intensity, $I_e$ is the equilibrium reflected light intensity, $A$ is the thin film surface area and $V$ is the injected vapor volume respectively. Adsorption rate $\left(\frac{dq_t}{dt}\right)$ was described as [49]:

$$\frac{dq_t}{dt} = aexp(-bq_t) \quad (2)$$

where $q_t$ is the quantity of gas adsorbed at time $(t)$, $a$ is the initial adsorption rate and $b$ is the Elovich desorption constant respectively. If $q_t$ was chosen as 0, Eq. (2) equals to $a$. If we chose the boundary conditions from $q_t = 0$ at t = 0 to $q_t = q_t$ at t = $t$, Eq. (2) can be easily integrated as [50]:

$$q_t = \left(\frac{1}{b}\right)ln(ab) + \left(\frac{1}{b}\right)lnt \quad (3)$$

Using Eq. (3), SPR experimental data can be fitted for the determination of Elovich constants $a$ and $b$. If we assume $t \gg t_0$, a plot of $q_t$ versus $lnt$ yields a linear relationship [51]. The Elovich model parameters $a$ and $b$ are calculated using the calculated $q_t$ values as a function of $lnt$ fitting graph.

## 3. Results and discussion

### 3.1. Synthesis

The step-by-step synthesis of asymmetric phthalocyanines (ZnPc1-$A_3B$, and ZnPc2-$AB_3$) was shown in Schemes 1 and 2 together with the reaction conditions. 4,5-bis(hexylthio)phthalonitrile (PN2) was synthesized and purified following previous work [52]. 4-(2-(2-ethoxyethoxy) ethoxy)phthalonitrile (PN1) was obtained by the aromatic nucleophilic substitution reaction of DEGME with 4-nitrophthalonitrilein the presence of $K_2CO_3$ and DMF (Scheme 1). The last step of the synthesis is template tetramerization of the substituted phthalonitrile in a high-boiling solvent using zinc acetate as a template agent.

Numerous asymmetric phthalocyanine derivatives with $A_3B/AB_3$ substitution patterns have been synthesized through the statistical cyclotetramerization of the phthalonitrile precursors PN1 (A) and PN2 (B) (Schemes 1 and 2) [53–58]. The ratio of these two precursors orients the proportion of the desired derivative. To promote the formation of the $A_3B/AB_3$ product, an excess of precursor A or B was used, respectively [59]. This approach ensures that the phthalocyanines formed predominantly consist of the symmetrical $A_4$ or $B_4$ derivatives together with the asymmetrical $A_3B/AB_3$ phthalocyanines. A 10:1 ratio of the starting materials was selected to favor the formation of these products, resulting almost exclusively in a mixture of symmetric $A_4/B_4$ and asymmetric $A_3B/AB_3$ phthalocyanines, as identified in our previous reports [52,60]. This 10:1 ratio was applied to a mixture of starting materials (PN1 and PN2), which underwent mixed cyclotetramerisation in the presence of zinc acetate in *n*-pentanol, and led to the phthalocyanines ZnPc1-$A_4$, ZnPc2-$B_4$, and ZnPc1-$A_3B$, ZnPc2-$AB_3$, separated by preparative thin layer chromatography. The reaction was successful as no other derivatives (except traces of $A_2B_2$ isomers) were observed, the symmetric phthalocyanines ZnPc1-$A_4$, ZnPc2-$B_4$ being obtained in 26% and 31% yield, and the asymmetric phthalocyanines ZnPc1-$A_3B$, ZnPc2-$AB_3$ in 14% and 16% yield, respectively, which are excellent for such asymmetrically substituted phthalocyanines.

At each step of the synthesis, both the structural integrity and the identity of the products were verified using spectroscopic analyses. All spectroscopic results are consistent with the proposed molecular structures (Figures S1-S12). The MALDI–MS spectra display intense molecular ion peaks at $m/z$ 1206.140 and 1407.047, confirming the formation of the ZnPc1-$A_3B$ and ZnPc2-$AB_3$, respectively. Their structural verifications were further achieved using both $^1H$ and $^{13}C$ NMR spectroscopy (Figures S7, S8, S11, S12). In comparison with their corresponding phthalonitrile precursors (PN1) (Figures S3, S4), the $^1H$ NMR signals of the phthalocyanines appear noticeably broadened. This broadening arises from the presence of multiple positional isomers that generate overlapping resonances, as well as from dynamic aggregation–disaggregation equilibria characteristic of phthalocyanine systems. Additionally, elemental analysis data for the PN1 and PN2 and the ZnPc1-$A_3B$ and ZnPc2-$AB_3$ were in close agreement with the corresponding theoretical values, further supporting the successful synthesis of the target compounds.

### 3.2. Photophysical and photochemical properties of asymmetric phthalocyanine derivatives

Phthalocyanines are highly π-conjugated macrocycles that display characteristic UV–Vis absorption profiles consisting mainly of Q and Soret (B) bands. The intense Q band, generally located between 650 and 750 nm, originates from HOMO–LUMO π→π* electronic transitions, whereas the Soret band appears in the near-UV region (300–350 nm) and is associated with higher-energy electronic excitations involving π→π* transitions. The aggregation behaviors of ZnPc1-$A_3B$ and ZnPc2-$AB_3$ structures were investigated by recording UV–Vis measurements, at a constant concentration (2 μM) in various organic solvents, including THF, DMF, toluene, dioxane (DIOX), $CHCl_3$, and DMSO (Fig. 2, Table S2). The compounds exhibited no significant solvatochromic shifts, with the Q-band positions remaining nearly constant across the different solvent environments. The lack of significant solvatochromism indicates that the electronic states of the core remain unaffected by solvent polarity. Moreover, the sharp and intense Q-bands across all solvents confirm that both complexes remain strictly monomeric at 2 μM, demonstrating excellent solubility and high stability against aggregate formation.

The electronic absorption spectra were recorded in THF at 2 μM-12 μM to verify their aggregation state. As illustrated in Figure S13, the Q-band intensities of both Pcs derivatives increased linearly with concentration, showing excellent correlation ($R^2$>0.998). This strict adherence to the Beer-Lambert law confirms that the ZnPcs derivatives exist predominantly as monomers within the studied range. Such observations underscore the high solubility and stability of structures against molecular association in organic media. The molar absorptivity coefficients (ε) were subsequently derived from the slopes of these regressions. The variations in the maximum absorbance wavelengths ($\lambda_{max}$), molar extinction coefficients (ε), and log ε values determined for the ZnPc1-$A_3B$ and ZnPc2-$AB_3$ in THF are summarized in Table 1.

The structural differences between the Pcs derivatives lead to notable shifts in their Q-band maxima, arising from the nature and number of the

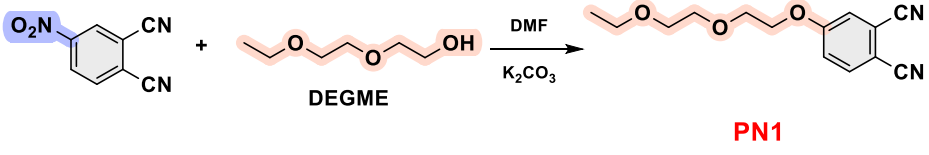


**Scheme 1.** The synthesis method of PN1.

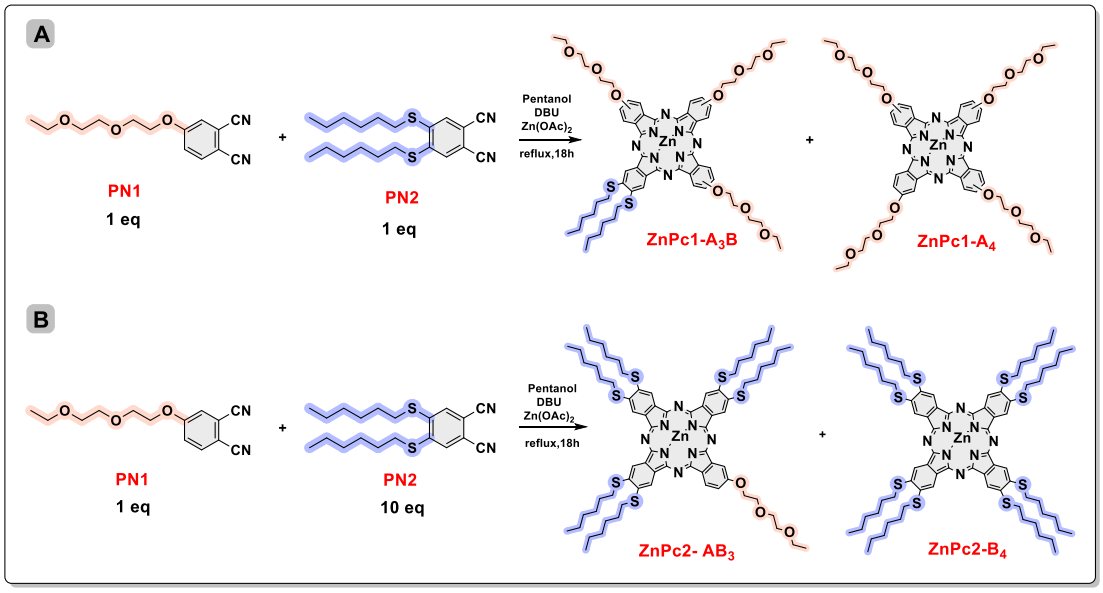


**Scheme 2.** The synthesis route of asymmetric phthalocyanine derivatives (ZnPc1-$A_3B$ (A) and ZnPc2-$AB_3$ (B)).

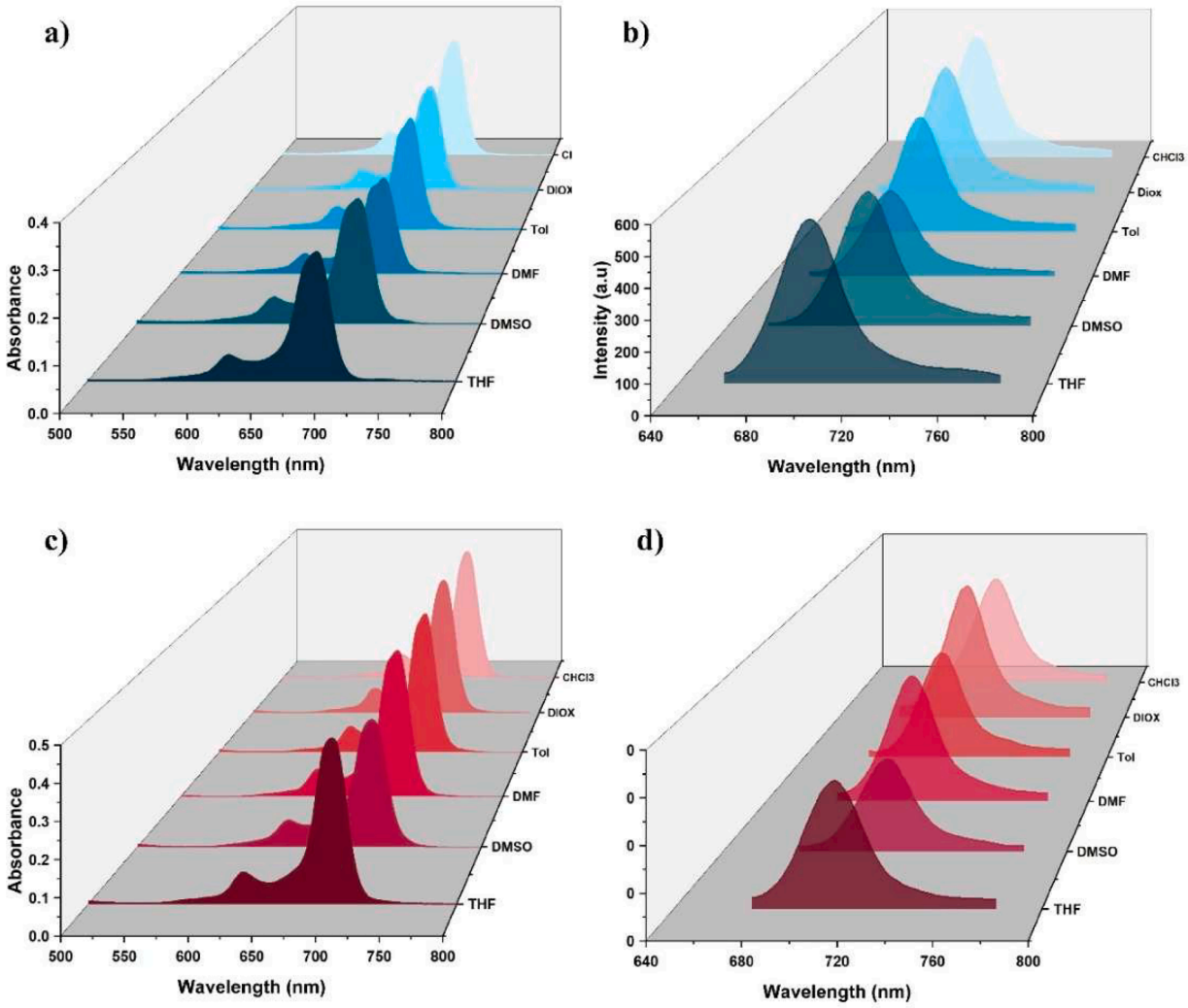


**Fig. 2.** Electronic absorption spectra of ZnPc1-$A_3B$ (a) and ZnPc2-$AB_3$ (c) in various organic solvents at a constant concentration of 2 μM. The fluorescence emission spectra for ZnPc1-$A_3B$ (b) and ZnPc2-$AB_3$ (d) recorded at the same concentration in the same solvent set.

**Table 1**
Maximum absorption wavelengths ($\lambda_{max}$), molar extinction coefficients (ε) and log ε values of the ZnPc derivatives in THF.

| Compound | $\lambda_{max}$ (nm) | ε (x10$^4$mol$^{-1}$cm$^{-1}$) | log ε |
|---|---|---|---|
| ZnPc1-$A_3$B | 687 | 12.3 | 5.09 |
| ZnPc2-$AB_3$ | 698 | 18.8 | 5.27 |

donor atoms bonded to the Pc-core. While both derivatives are asymmetric, ZnPc1-$A_3$B features three oxygen (O) and two sulfur (S) donor-bonded groups, whereas ZnPc2-$AB_3$ is substituted with one O-bonded and six S-bonded functional groups. The higher degree of S-substitution in ZnPc2-$AB_3$ enhances the electron density of the macrocyclic ring more effectively than O-donors, thereby narrowing the HOMO-LUMO energy gap. Compared with ZnPc1-A3B, the Q band of ZnPc2-AB3 was shifted bathochromically by 11 nm.

As illustrated in Fig.s 2a and 2d, the fluorescence spectra were recorded at a constant concentration in various solvents to evaluate the photophysical profiles of the complexes. Consistent with the electronic absorption data, the fluorescence spectra showed no significant solvatochromic shifts. This indicates that both the ground and emissive states of the compounds remain relatively unaffected by solvent polarity. Table 2 summarizes the maximum absorption and emission wavelengths, along with the Stokes shifts. Despite minor fluctuations in their absorption maxima, both ZnPc1-$A_3$B and ZnPc2-$AB_3$ exhibited highly consistent photophysical behavior across all studied solvent environments.

The fluorescence quantum yields ($\Phi_F$) of the ZnPcs were determined by the relative method using unsubstituted zinc phthalocyanine (unSub-ZnPc) as the standard (Figures S14 and S15). The technical details and the equation used for the relative method are provided in Supporting Information Section S2. The results, along with fluorescence lifetimes ($\Gamma_F$) and singlet oxygen yields ($\Phi\Delta_S$), are detailed in Table 2 (Figure S16). ZnPc1-$A_3$B and ZnPc2-$AB_3$ exhibited relatively similar fluorescence quantum yields of 0.22 and 0.26, respectively. The minor variation shows that the number of sulfur and oxygen donor atoms does not lead to a drastic change in the radiative decay pathways. The slightly shorter fluorescence lifetime of ZnPc2-$AB_3$ (2.31 ns) compared to ZnPc1-$A_3$B (2.61 ns) is consistent with the minor narrowing of the HOMO–LUMO gap.

Furthermore, singlet oxygen quantum yields ($\Phi_{\Delta S}$) and fluorescence lifetime ($\Gamma_F$) measurements were determined using a Horiba Jobin Yvon Fluorolog-3 spectrophotometer. The singlet oxygen yields, determined by the direct method using unSub-ZnPc as the reference, were found to be 0.74 and 0.72 for ZnPc1-$A_3$B and ZnPc2-$AB_3$, respectively (Figure S16). These high and comparable values show that both derivatives remain highly efficient photosensitizers, regardless of the specific substitution pattern of the O- and S-donor groups.

### 3.3. Mesogenic properties of asymmetric phthalocyanine derivatives

The thermotropic liquid crystalline properties of the asymmetric phthalocyanine derivatives were characterized using polarizing optical microscopy (POM), thermogravimetric analysis (TGA), differential scanning calorimetry (DSC), and X-ray diffraction (XRD) techniques. Both compounds exhibited thermotropic columnar mesophases. During POM analysis, the birefringent textures remained unchanged throughout the heating process from 25 to 300°C, indicating high mesophase stability. Characteristic optical textures associated with discotic columnar liquid crystalline phases were clearly observed for both ZnPc derivatives (Fig. 3). In addition, no visually detectable thermal decomposition occurred during the microscopic investigations of both ZnPc derivatives.

The mesophases were identified by XRD measurements performed at room temperature. Chloroform solutions of compounds ZnPc1-$A_3$B and ZnPc2-$AB_3$ were drop-cast onto glass substrates and allowed to evaporate under ambient conditions. The resulting powder XRD patterns exhibit characteristic reflections of columnar mesophases commonly observed for substituted phthalocyanines (Figure S17, Table S3). In the low-angle region ($2\theta = 4°–6°$), both derivatives display a sharp primary reflection accompanied by either a shoulder or a weak additional peak. According to literature reports, the splitting of the (10) reflection of a hexagonal columnar phase ($Col_h$) into the (11) and (20) reflections is indicative of a rectangular columnar phase ($Col_r$) [25,63]. The lattice parameters *a* and *b* were calculated using the relation $1/d^2_{hkl} = h^2/a^2 + k^2/b^2$. On this basis, a plausible indexation of the $Col_r$ mesophase was established, as summarized in Table S3. These findings indicate the formation of a two-dimensional rectangular lattice in which disc-like phthalocyanine molecules stack into columns arranged in a rectangular geometry (Fig. 3). ZnPc2-$AB_3$ was thus assigned to a $Col_r$ mesophase with *P2gg* symmetry. In contrast, in the low-angle region, ZnPc1-$A_3$B exhibits sharp diffraction peaks with spacing ratios of 1: $1/\sqrt{3}$: $1/\sqrt{4}$: 1…, which are characteristic of a hexagonal columnar mesophase [64] (Table S3). Together with the observed liquid crystalline texture, these results indicate the formation of a two-dimensional hexagonal lattice in which disc-like ZnPc1-$A_3$B molecules stack into columns arranged in a hexagonal geometry. The texture of ZnPc1-$A_3$B is similar to the texture described in the literature for other metal phthalocyanines, forming a discotic hexagonal mesophase ($Col_h$) (Fig. 3a) [65–68].

**Table 2**
Photophysical and photochemical parameters of ZnPc compounds determined in THF.

| Compound | $\lambda_{abs}^{max}$ (nm) | $\lambda_{em}^{max}$ (nm) | $\Phi_F$ | $\Phi\Delta_S$ | $\Gamma_F$ (ns) |
|---|---|---|---|---|---|
| ZnPc1-$A_3$B | 687 | 698 | 0.22 | 0.74 | 2.61 |
| ZnPc2-$AB_3$ | 698 | 710 | 0.26 | 0.72 | 2.31 |
| unSub-ZnPc | 666 | 673 | 0.25[61] | 0.53[62] | - |

### 3.4. SPR curves of ZnPc1-$A_3$B and ZnPc2-$AB_3$ thin films; characterization and dichloromethane sensing

SPR curves of uncoated gold, ZnPc1-$A_3$B, and ZnPc2-$AB_3$ thin films were obtained before and after the heating process and presented in Fig. 4.

Compared to the bare gold substrate on which no thin film was produced, the SPR curves of the ZnPc1-$A_3$B thin film indicate an angle of shift, which proves thin film formation. The SPR ($\theta_{SPR}$) angle of the bare gold layer occurred at a value of $44.04^0$. The SPR ($\theta_{SPR}$) angles of the ZnPc1-$A_3$B and ZnPc2-$AB_3$ thin films reached a larger value, as expected with thin film production. The amount of angle shifts $\Delta\theta$ ($^0$) during thin film production compared to the bare gold layer was given in Table 3 separately before and after the heating process. It is observed that the surface plasmon resonance angle value decreased for all thin films during the heating process. SPR curves and the WINSPALL fitting data for the ZnPc2-$AB_3$ thin film are presented in Figure S18. Using these SPR curves and a WINSPALL fitting software, the optical constants of both thin films were determined before and after heating. Results were summarized in Table 3.

Fig. 5 shows the SPR curves of the ZnPc1-$A_3$B thin film sensor during exposure and unexposure to DCM vapor. The SPR curves of the ZnPc2-$AB_3$ thin film sensor were presented in Figure S19. Both thin film sensors have a change in the resonance angle that is obvious when DCM vapor was introduced into the gas cell. After flashing dry air into the gas cell, DCM vapor was removed from the ZnPc1-$A_3$B and ZnPc2-$AB_3$ thin film sensors because the angle shift came back to its initial value. These results proved that the ZnPc1-$A_3$B and ZnPc2-$AB_3$ thin film sensors yielded reversible responses to DCM vapor. The resonance angle value its change during interaction with the DCM vapor were stated in Table 4 separately for the thin films before and after heating.

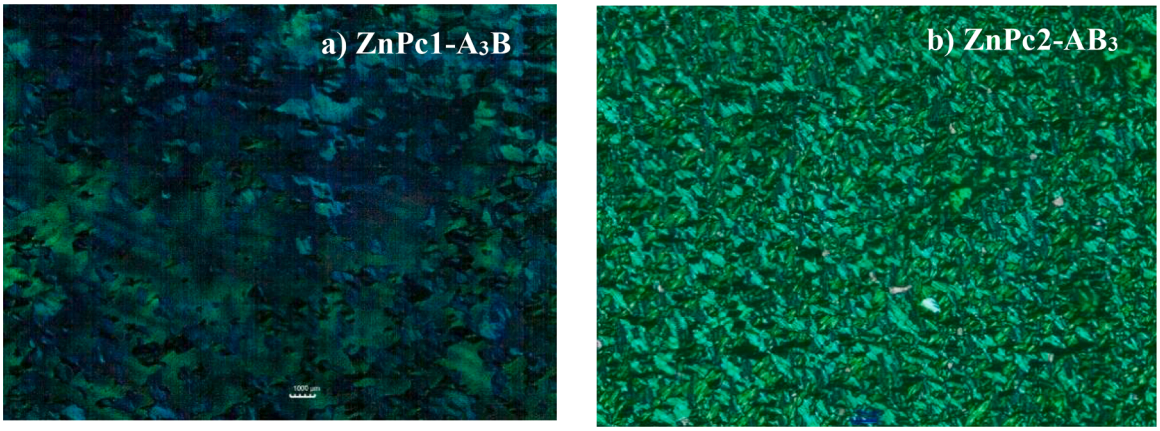


**Fig. 3.** POM images of compounds a) ZnPc1-$A_3B$ and b) ZnPc2-$AB_3$ (50X magnification).

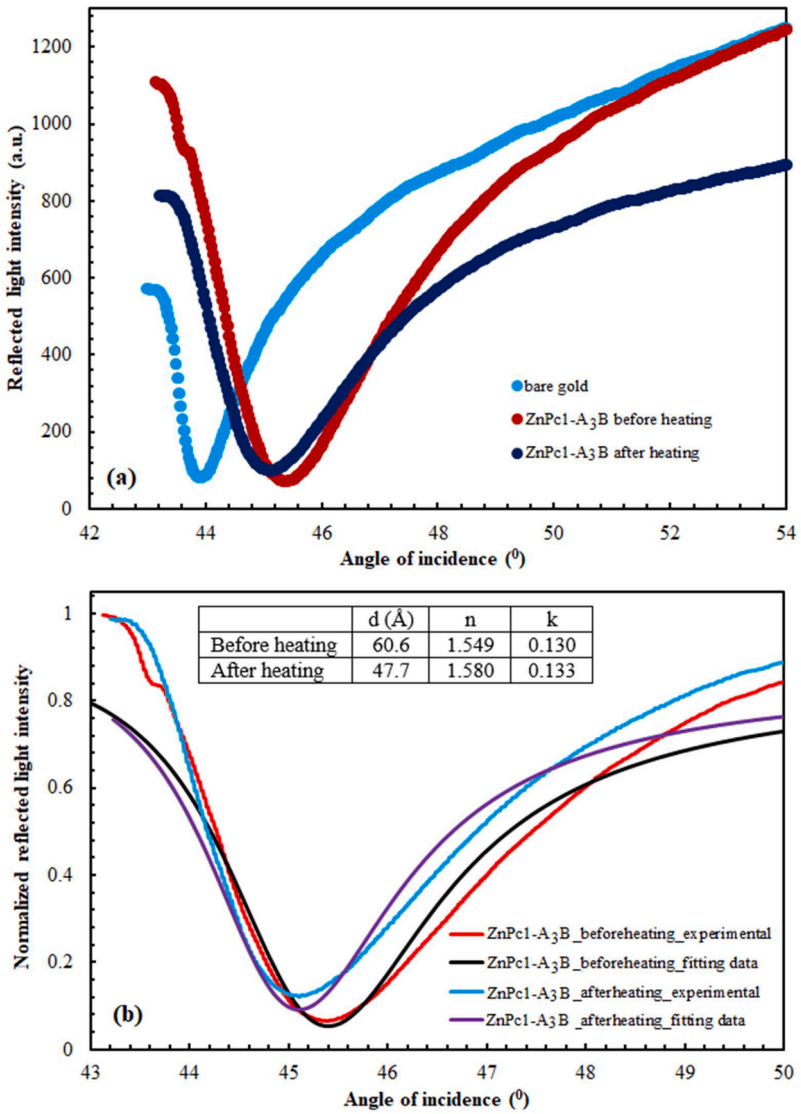


**Fig. 4.** SPR curves of a) bare gold, ZnPc1-$A_3B$ thin film before and after heating. b) WINSPALL fitting data, including the estimated values of the thickness and the optical constants.

**Table 3**
SPR results and optical constants of thin films.

| Thin film | before heating | | after heating | | Optical constants calculated from WINSPALL fitting software | | | | | | Reference |
|---|---|---|---|---|---|---|---|---|---|---|---|
| | $\theta_{SPR}$ ($^0$) | Δθ ($^0$) | $\theta_{SPR}$ ($^0$) | Δθ ($^0$) | before heating | | | after heating | | | |
| | | | | | d (nm) | N | k | d (nm) | n | k | |
| ZnPc1-$A_3B$ | 45.39 | 1.35 | 45.1 | 1.06 | 60.6 | 1.54 | 0.13 | 47.7 | 1.58 | 0.1328 | This study |
| ZnPc2-$AB_3$ | 45.05 | 1.01 | 44.95 | 0.91 | 48.6 | 1.52 | 0.1238 | 31.1 | 1.54 | 0.146 | |
| ZnPc2-$B_4$ | 45.06 | 1.02 | 44.96 | 0.92 | 49.5 | 1.52 | 0.1154 | 43.5 | 1.54 | 0.1286 | [37] |

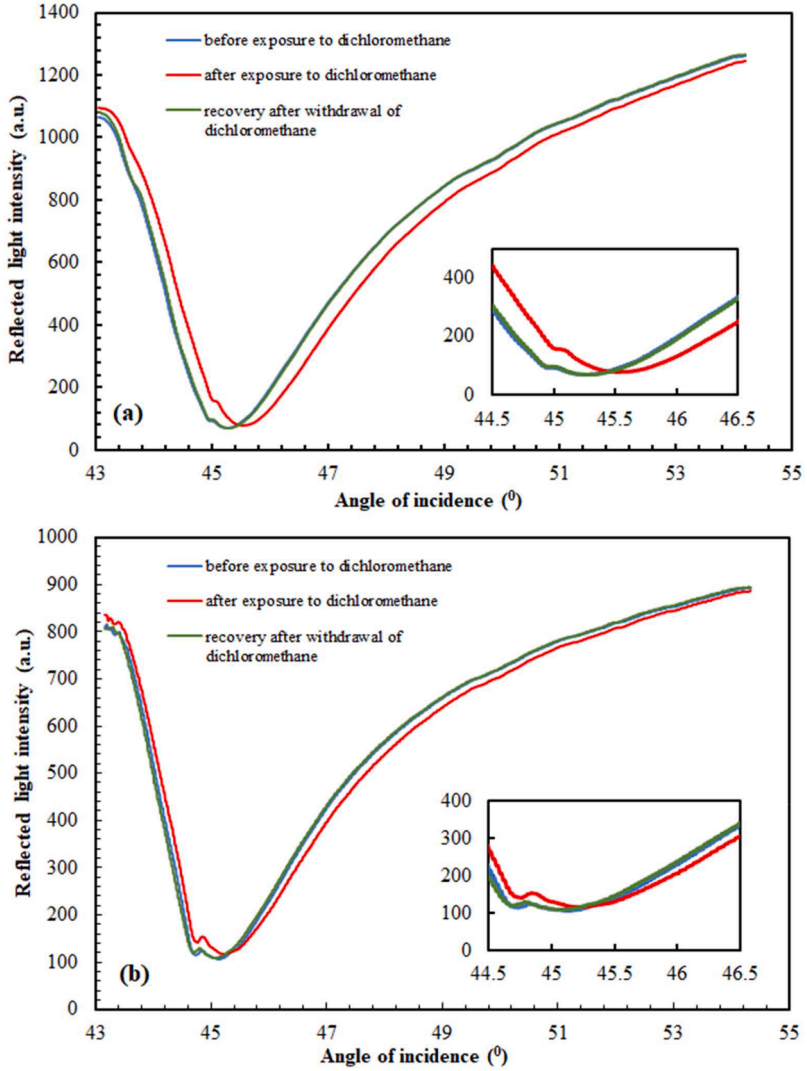


**Fig. 5.** The SPR curves of the ZnPc1-$A_3B$ thin film sensor. Inset in the figure provides a close look at the SPR minimum value.

**Table 4**
Δθ values of the ZnPc1-$A_3B$ and ZnPc2-$AB_3$ thin film sensors on exposure.

| Thin Film | before heating $\theta_{SPR}$ ($^0$) | Δθ ($^0$) due to exposure of DCM vapor | after heating $\theta_{SPR}$ ($^0$) | Δθ ($^0$) due to exposure of DCM vapor | Reference |
|---|---|---|---|---|---|
| ZnPc1-$A_3B$ | 45.26 | 0.26 | 45.13 | 0.10 | This study |
| ZnPc2-$AB_3$ | 44.98 | 0.1 | 44.68 | 0.06 | |
| ZnPc2-$B_4$ | 45.05 | 0.09 | 44.96 | 0.05 | [37] |

### *3.5. Responses of the ZnPc1-$A_3B$ and ZnPc2-$AB_3$ thin film based SPR optical sensors*

The interactions between thin film sensors and DCM vapor caused changes in the reflected light intensity due to the additional adsorbed vapor molecules, which resulted in changes in the refractive index and thickness of the thin film. The reflected light intensity difference (ΔI) between the baseline value ($I_0$) and the equilibrium value (I) after vapor interaction was used to define the sensor response, which is presented in Eq. (5) as follows;

$$\Delta I = I - I_0 \quad (4)$$

sensor response (%)=($\Delta I/I_0$)x100 (5)

To accurately represent the variability of the results, the SPR measurement data to selected vapor was analyzed using the mean value ($\overline{SR\%}$) and the standard deviation ($\sigma$). They were calculated using following equations as [69]:

$$\overline{SR\%} = \frac{\sum_{i=1}^{n}(SR\%)_i}{n} \pm \sigma \quad (6)$$

where n is the number of cycles. $\sigma$ is given as:

$$\sigma = \sqrt{\frac{\sum_{i=1}^{n}((SR\%)_i - \overline{SR\%})^2}{(n-1)}} \quad (7)$$

The SPR dynamic responses of the ZnPc1-$A_3$B and ZnPc2-$AB_3$ thin film sensors before and after heating were recorded by collecting the reflected light intensity data against time at a constant angle, when they were exposed to the DCM vapor. To monitor the concentration dependence behavior of these thin film sensors, a 5 mL syringe was used to introduce the vapor into the gas cell with the concentration vapor/air ratio of 25, 50, 75, and 100% within a 2 min time period. Fig. 6 gives the concentration dependence responses of the ZnPc1-$A_3$B and ZnPc2-$AB_3$ thin film sensors before and after heating.

The results show that the sensor responses increase rapidly with the injection of the DCM vapor and reach the equilibrium state after a while, and it returns to the baseline value in time after exposure to dry air. When the concentration of the vapor was increased, the ZnPc1-$A_3$B and ZnPc2-$AB_3$ thin film sensor responses were also increased. Additionally, the sensor responses before heat treatment are higher than the sensor responses after heat treatment. According to Fig. 7, the ZnPc1-$A_3$B thin film sensor before the heat treatment has much higher responses to DCM vapor compared to the ZnPc2-$AB_3$ thin film sensor. After heating process, both sensor responses were reduced due to film thickness changes.

The results show a gradual increase in both sensor responses with increasing DCM concentration. This is due to the adsorption and/or diffusion of a larger number of vapor molecules on the surface of the thin film sensor at higher concentrations. The maximum sensing response of the ZnPc1-$A_3$B thin film sensor can be clarified by the highest film thickness and refractive index of this thin film sensor compared with the other thin film sensors.

### 3.6. *Reversibility, repeatability, and response/recovery times of ZnPc1-$A_3$B and ZnPc2-$AB_3$ spun thin films*

Reproducibility and reversibility are two other important parameters for evaluating vapor sensor applications. To test these parameters, the dynamic time-dependent SPR response of each thin film sensor has been repeated for three sequential cycles at 100% saturated concentration value for the DCM vapor (Fig. 7). The results for both thin film sensors

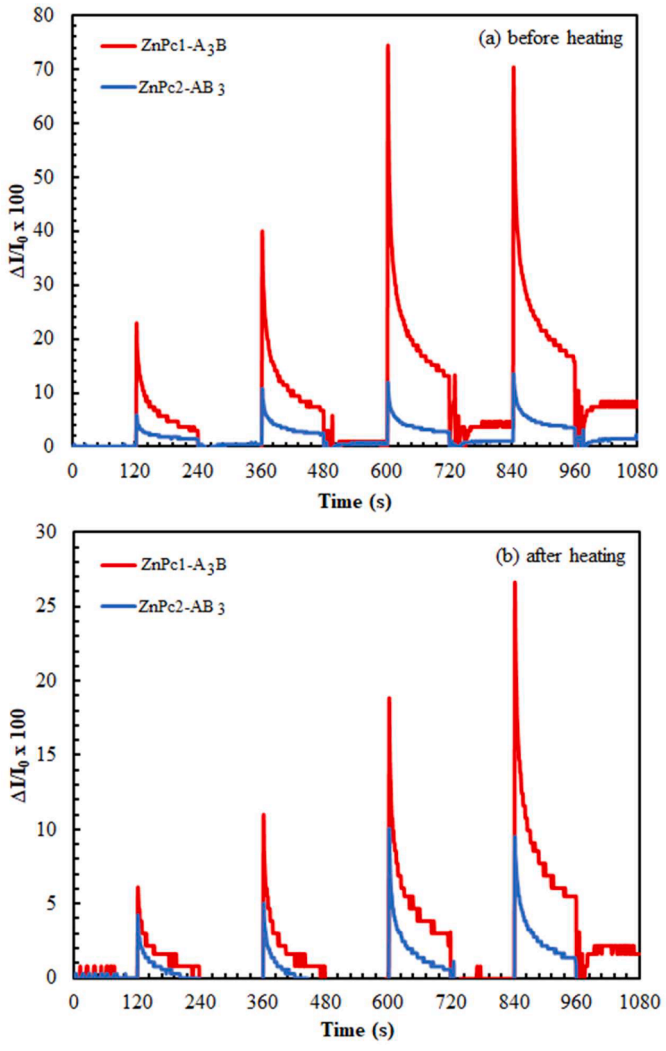


**Fig. 6.** Time-dependent dynamic SPR response of thin film sensors at different concentration values: a) before heating b) after heating.

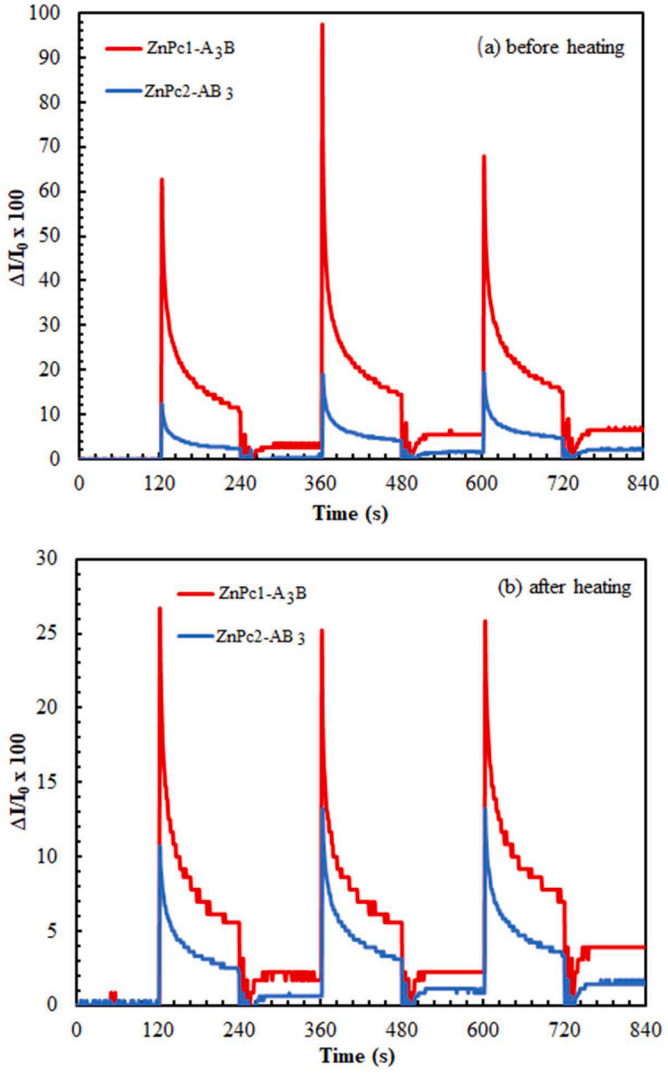


**Fig. 7.** Reproducibility, stability, and sensitivity measurements of the thin film sensors a) before heating b) after heating.

show that after the injection of the analyte and its absorption by the sensor and vapor discharge, the sensors' response almost returns to its baseline state, indicating that the sensors were fully reversible. Besides, the results show that the responses were almost equal for three repeated cycles, which validates the repeatability of both thin film sensors.

The response time is defined as the time taken for the sensors' response to reach 90% of its maximum signal value, and the recovery time is the time for the sensor response to decrease to 10% of the equilibrium baseline value [70–72]. For three successive cycles, the ZnPc1-$A_3$B and ZnPc2-$AB_3$ thin film sensor responses were similar under the same concentration value, with no significant changes in response and recovery times. The sensor response time to reach 90% of the equilibrium value when the sensor was exposed to the DCM vapor at 100% concentration was determined as an average value of response time (1–2 s before-after heating treatment respectively) and an average value of recovery time (8–10 s before and 7–10 s after heating treatment) for both thin film sensors during three cycles. It can be concluded that both proposed thin film sensors have relatively fast response and recovery times. Similar results have been reported for the symmetrical ZnPc2-$B_4$ thin film sensor [37].

### 3.7. Calibration curves for ZnPc1-$A_3$b and ZnPc2-$AB_3$ spun thin films, sensitivity, limit of detection and limit of quantification

Fig. 7 shows the ZnPc1-$A_3$B and ZnPc2-$AB_3$ thin film sensor responses before and after the heating process versus DCM concentrations. Linear relationships between sensor responses and DCM vapor concentration values were observed, and the slope of this linear relationship was used to calculate the sensor sensitivity. Other important parameters that can affect the sensors' performance are limit of detection (LOD) and limit of quantification (LOQ). In general, the LOD value is the lowest amount of an analyte that can be detected by a sensor. The LOQ value is the lowest concentration of an analyte that can be consistently measured with respectable precision and accuracy [73,74]. LOD and LOQ values of both thin film sensors before and after heating treatment were calculated using Eqs. 8 and 9 [75,76]:

$$LOD = \frac{3.3\sigma}{S} \tag{8}$$

$$LOQ = \frac{10\sigma}{S} \tag{9}$$

where σ is the standard deviation (0.001), and S represents the sensitivity of the sensor that is calculated via the linear slope of the calibration curve presented in Fig. 8. σ was calculated using blank signal data taken at 1-second intervals between 1 and 120 s for baseline noise. All sensor parameters were presented in Table 5.

Sensitivity values, which are represented as (% response) per ppm of the DCM vapor concentration, were calculated using the linear dependence shown in Fig. 8. The highest sensitivity before and after the heating treatment was calculated for the ZnPc1-$A_3$B thin film sensor in this work. All sensitivity values before the heating treatment were higher than after the heating treatment. It is very clear that heating the thin film sensor reduced the sensor sensitivity. Another important result is that the ZnPc1-$A_3$B thin film sensor yielded significantly the highest sensitivity values compared with the ZnPc2-$AB_3$ and ZnPc2-$B_4$ thin film sensors, as well as the lowest LOD and LOQ values compared with those of the ZnPc2-$AB_3$ and ZnPc2-$B_4$ thin film sensors.

To properly contextualize the selectivity claims and assess the practical utility of the sensors for environmental monitoring, measurements of two non-chlorinated volatile organic compounds, such as toluene and ethanol, were included, along with comparative SPR response data. 3 reciprocal exposures to saturated ethanol and toluene vapors were tested, and the SPR kinetic experimental results were presented in Fig.s 9 and 10 for both as prepared thin films and the heat-threated thin films after the heating process.

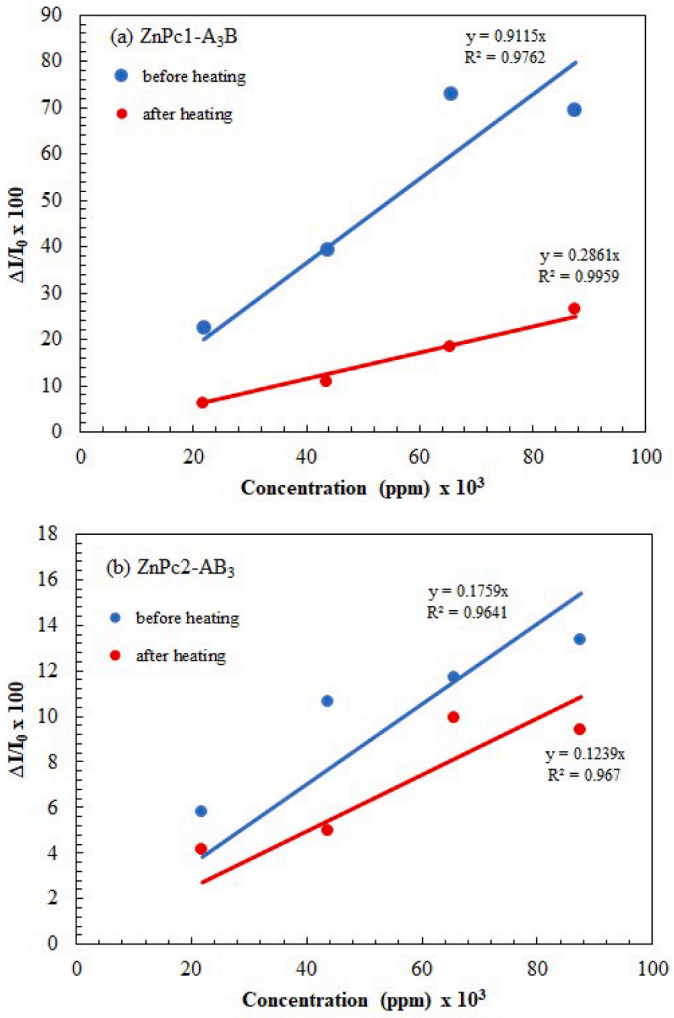


**Fig. 8.** The calibration curves to determine the S, the LOD and the LOQ of the a) ZnPc1-$A_3$B and b) ZnPc2-$AB_3$ thin film sensors.

It was observed that for all cases, both thin films exhibited the highest amount of sensor response to dichloromethane vapor compared with ethanol and toluene vapors. ZnPc1-$A_3$B and ZnPc2-$AB_3$ thin-film sensors can be labelled as selective for dichloromethane vapor among the tested vapors. Table 6 gives the statistical analysis from at least three replicate measurements. These results demonstrated that the observed SPR signal enhancement is specific to dichloromethane interactions and is merely a general response to vapor-induced refractive index changes.

For the long-term stability test, 10 cycles of exposure to saturated dichloromethane vapor to the ZnPc1-$A_3$B thin film sensor were performed, and the result was presented in Fig. 11.

It was observed that the sensor gives a stable response through 10 cycles in terms of the sensor response value. Sensor parameters such as response and recovery times were also shown to be stable over 10 cycles of exposure.

### 3.8. The Elovich model fitting results

From the SPR kinetic graph for ZnPc1-$A_3$B and ZnPc2-$AB_3$ thin film sensors in Fig. 7, the 120–240 s time interval was selected as cycle 1, the 360–480 s time interval as cycle 2, and the 600–720 s time interval as cycle 3. Using each cycle's data and Eq. (1), $q_t$ was calculated. The changes of $q_t$ versus t and ln t for the ZnPc1-$A_3$B thin film sensor before and after the heating process were given in Fig.s 12 and S20 respectively. Similar calculations were repeated for the ZnPc2-$AB_3$ thin film

**Table 5**
Sensor parameters of the ZnPc1-$A_3B$ and ZnPc2-$AB_3$ thin films.

| ZnPc thin film exposed to DCM vapor | | Sensitivity x $10^{-3}$ (% response/ppm) | LOD (ppm) | LOQ (ppm) | Reference |
|---|---|---|---|---|---|
| ZnPc1-$A_3B$ | Before heating | 0.9115 | 3.62 | 10.97 | This study |
| | After heating | 0.2861 | 11.53 | 34.95 | |
| ZnPc2-$AB_3$ | Before heating | 0.1759 | 18.76 | 56.85 | |
| | After heating | 0.1239 | 26.63 | 80.71 | |
| ZnPc2-$B_4$ | Before heating | 0.2849 | 11.58 | 35.10 | [37] |
| | After heating | 0.1213 | 27.20 | 82.44 | |
| Pillar[5]arene derivatives thin films | P [5] 1 | 0.483 | 6.83 | 20.69 | [77] |
| | P [5] 2 | 0.225 | 14.68 | 44.48 | |
| Pillar[6]arene thin films | | 0.2614 | 1.26 | 3.825 | [78] |
| π–π* complexes thin films | PHENPc | 0.0007 | 4714 | 14.286 | [79] |
| | ANTPc | 0.005 | 660 | 2000 | |
| | PRYPc | 0.006 | 550 | 1667 | |
| Calix[4]resorcinarenes thin films | FC 1 | 0.115 | 28.69 | 86.95 | [80] |
| | FC 2 | 0.084 | 39.29 | 119.04 | |
| PMMA/UiO-66-NH2@PMMA MOF thin films | pure PMMA | 0.117 | 25.68 | Not reported | [81] |
| | UiO-66-NH2@PMMA | 0.043 | 69.76 | Not reported | |

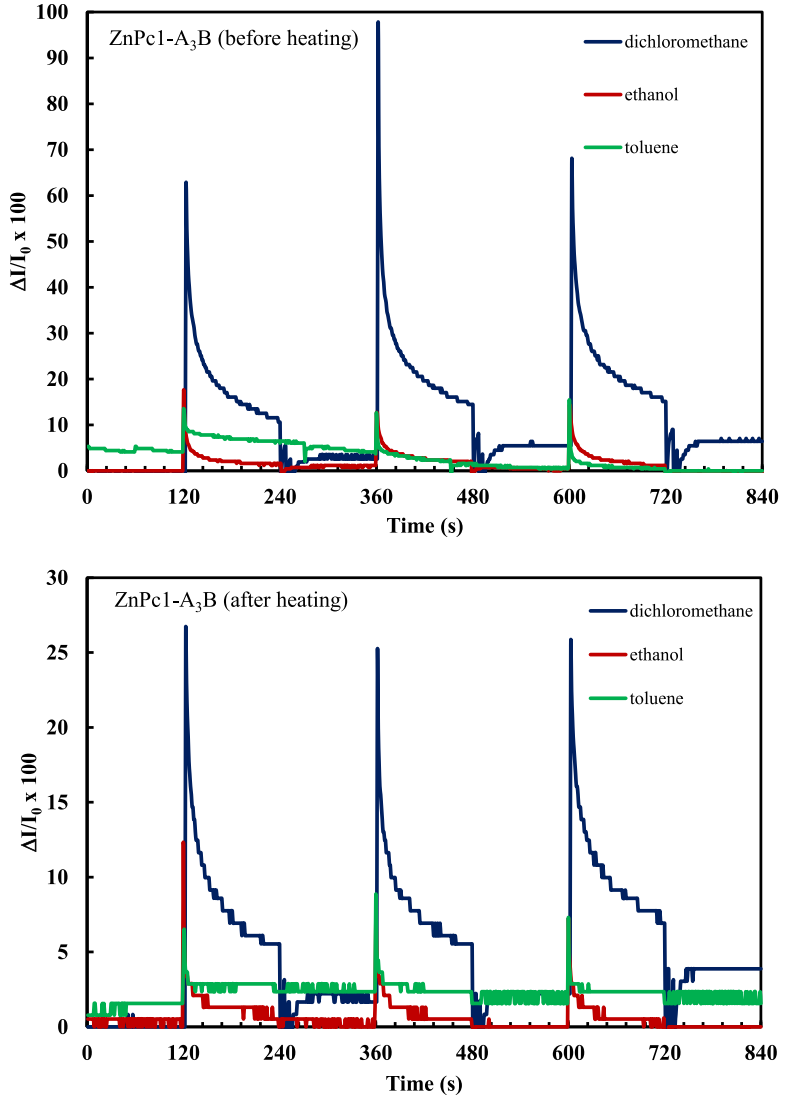


**Fig. 9.** Sensor response of the ZnPc1-$A_3B$ thin film before and after heating towards saturated concentrations of dichloromethane and toluene vapors.

sensor before and after heating processes, which were given in Figures S 21 and S22. Using Eq. (3), and Figs. (12, S20-22), *a*, *b* and $R^2$ parameters for each cycle of ZnPc1-$A_3B$ and ZnPc2-$AB_3$ thin film sensors were calculated for DCM vapor. These values were summarized in Table 7.

Table 7 shows the Elovich constants (a and b), their mean values, and standard deviations that were calculated for each cycle of the DCM vapor to which the ZnPc1-$A_3B$ and ZnPc2-$AB_3$ thin film sensors were exposed. The mean value of the initial adsorption rate (a) for both thin

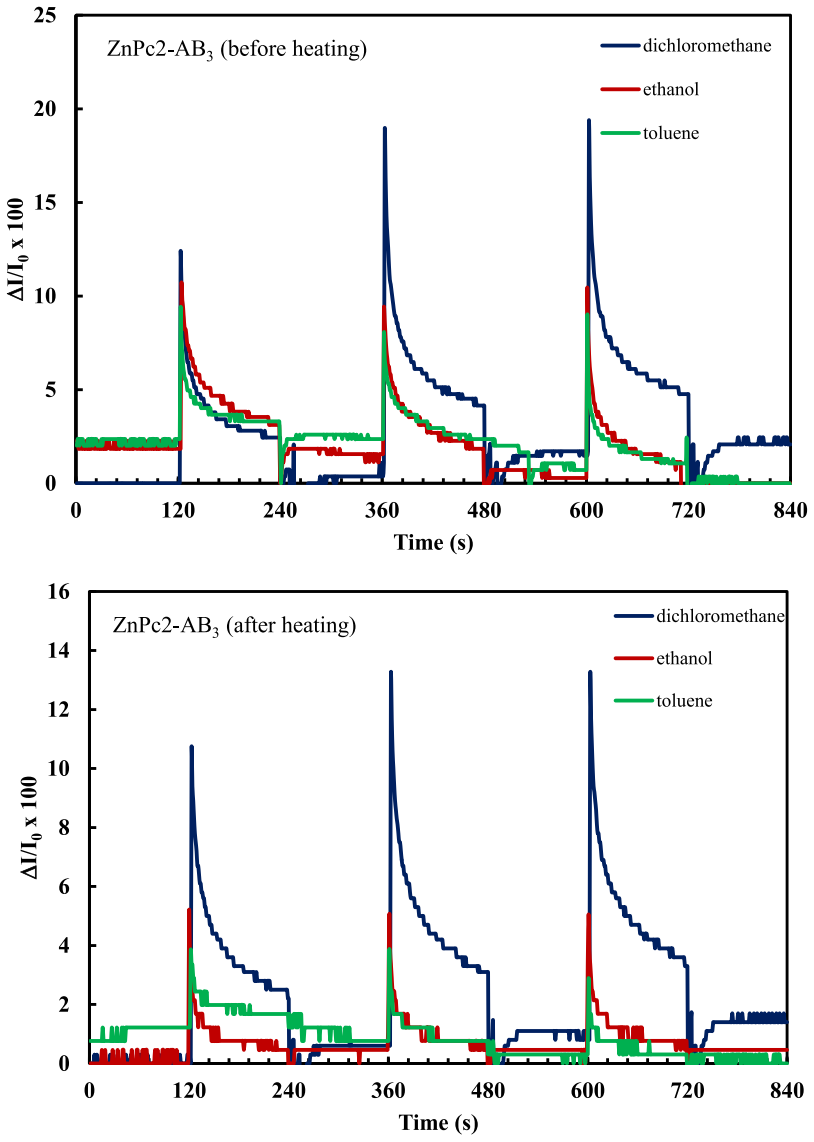


**Fig. 10.** Sensor response of the ZnPc2-$AB_3$ thin film before and after heating towards saturated concentrations of dichloromethane and toluene vapors.

**Table 6**
The statistical analysis of three replicate measurements.

| Thin Film | Vapor | Run (cycle) | ***SR***% | | The mean value $\overline{SR}$% | | Standard Deviation σ | |
|---|---|---|---|---|---|---|---|---|
| | | | Before heating | After heating | Before heating | After heating | Before heating | After heating |
| ZnPc1-$A_3B$ | DCM | 1 | 61.736 | 26.315 | 74.49 | 25.48 | 17.82 | 0.83 |
| | | 2 | 94.855 | 24.653 | | | | |
| | | 3 | 66.881 | 25.484 | | | | |
| ZnPc2-$AB_3$ | DCM | 1 | 12.210 | 10.600 | 16.64 | 12.26 | 3.84 | 1.44 |
| | | 2 | 18.681 | 13.100 | | | | |
| | | 3 | 19.047 | 13.100 | | | | |
| ZnPc1-$A_3B$ | Toluene | 1 | 13.421 | 6.527 | 13.86 | 6.35 | 1.45 | 1.05 |
| | | 2 | 12.684 | 5.221 | | | | |
| | | 3 | 15.486 | 7.310 | | | | |
| ZnPc2-$AB_3$ | Toluene | 1 | 9.208 | 3.810 | 8.65 | 3.50 | 0.67 | 0.52 |
| | | 2 | 7.910 | 3.810 | | | | |
| | | 3 | 8.854 | 2.896 | | | | |
| ZnPc1-$A_3B$ | Ethanol | 1 | 17.109 | 12.335 | 14.69 | 8.83 | 2.23 | 3.03 |
| | | 2 | 12.684 | 7.086 | | | | |
| | | 3 | 14.306 | 7.086 | | | | |
| ZnPc2-$AB_3$ | Ethanol | 1 | 10.623 | 5.052 | 10.05 | 5.05 | 0.64 | 0.001 |
| | | 2 | 9.348 | 5.050 | | | | |
| | | 3 | 10.198 | 5.053 | | | | |

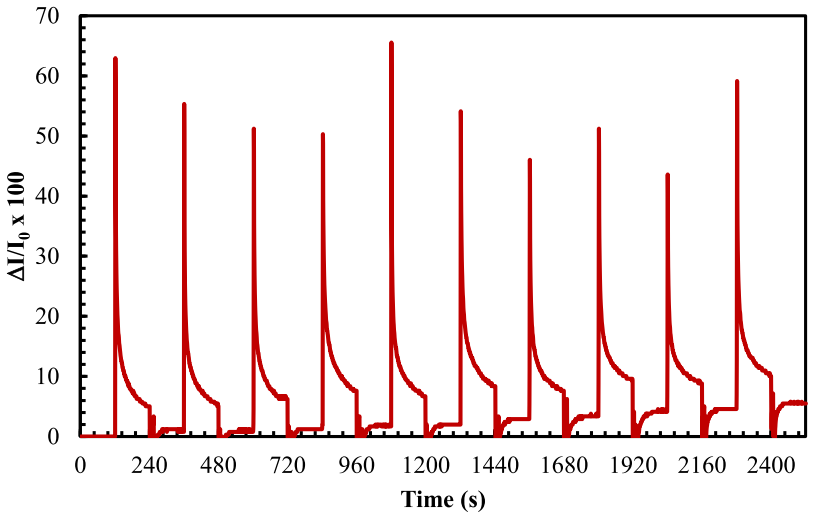


**Fig. 11.** 10 cycles of exposure to saturated dichloromethane vapor of spun ZnPc1-$A_3B$ thin film sensor.

films before the heating process is higher than the mean value of a value after the heating process. Similar results are seen, where the values for the ZnPc1-$A_3B$ thin film are higher than the values for the ZnPc2-$AB_3$ thin film. $R^2$ values were found to be in the range of 0.95–0.99, which shows fitting results are in very good agreement.

### *3.9. Influence of chemical structure on sensor sensitivity in the liquid-crystalline octakis(hexylthio)zinc(II) phthalocyanine spun thin films*

Previous studies have suggested that metallophthalocyanines possess two principal adsorption sites for gas molecules: the central metal ion and the conjugated π-electron macrocyclic system [47,82,83]. In substituted phthalocyanines, the peripheral substituents act as additional adsorption sites. Based on our previous studies and Raman spectral comparisons of phthalocyanine films before and after VOC exposure, saturated compounds such as ethanol and chloroform predominantly interact through hydrogen-bonding between the electron-donor atoms (O or Cl) of the analytes and the hydrogen atoms of the alkyl or polyoxoethylene substituents. In contrast, VOC vapors containing π-bonds mainly interact with the phthalocyanine layer via π–π stacking with the conjugated macrocyclic system [84,85]. Accordingly, the sensor responses observed for the ZnPc1-$A_3B$ and ZnPc2-$AB_3$ derivatives toward DCM may be associated with intermolecular interactions between dichloromethane molecules and the polyoxoethylene and alkylthio substituents present in these structures. Although non-clasical hydrogen-bonding may contribute to the adsorption process, direct experimental evidence confirming the nature of these interactions was not obtained in the present study.

In our previous study, ZnPc2-$B_4$, bearing eight alkylthia chains, was employed to fabricate spin-coated thin films, and its vapor sensing properties toward various organic vapors were investigated [37]. Following the promising sensor performance obtained from this compound, two novel asymmetric phthalocyanine molecules, ZnPc1-$A_3B$ and ZnPc2-$AB_3$, were subsequently designed and synthesized to enhance sensing performance.

These asymmetric ZnPc derivatives contain different numbers of polyoxyethylene and alkylthia substituents attached to the ZnPc macrocycle, resulting in variations in the number of oxygen and sulfur atoms within their side chains. The sensor sensitivities, as well as the calculated LOD and LOQ values, indicate that increasing the number of polyoxyethylene side chains is associated with improved sensor performance. Specifically, the ZnPc1-$A_3B$ thin film (before heating) exhibited the highest sensitivity (0.9115 response/ppm) and the lowest LOD value (3.62 ppm) among all measurements. Moreover, compared to ZnPc2-$AB_3$ thin film (before the heating) which showed a considerably higher LOD value (18.76 ppm), suggests that the larger number of oxygen atoms present in the polyoxyethylene groups may contribute to enhanced analyte uptake and sensing behavior. Nevertheless, the specific molecule analyte interactions for this trend were not directly investigated in the present study and therefore require further experimental investigation.

As known, the nature of the peripheral substituents play a significant role in determining the sensing behavior of phthalocyanine thin films toward chlorinated solvents. Phthalocyanine containing polyoxyethylene side chains (ZnPc1$A_3B$) generally exhibit enhanced responses to DCM due to the presence of multiple oxygen atoms, which increase polarity and promote stronger interactions with the analyte molecules. In addition, the flexible polyoxyethylene groups can facilitate analyte diffusion within the sensing layer, leading to a more pronounced modulation of the electrical properties. In contrast, alkylthia substituents for ZnPc2-$AB_3$ mainly contribute to structural stability and intermolecular packing, but their relatively hydrophobic character may limit analyte uptake and result in a comparatively weaker sensing signal.

Considering the liquid crystalline properties, it is observed that the two phthalocyanine derivatives exhibit different mesophases; columnar hexagonal ($Col_h$) for ZnPc1-$A_3B$ and columnar rectangular ($Col_r$) for ZnPc2-$AB_3$. ZnPc1-$A_3B$ exhibiting a $Col_h$ mesophase demonstrates superior sensing performance compared to ZnPc2-$AB_3$ possessing a $Col_r$ mesophase. This difference may be attributed to the distinct liquid crystalline organizations of the two phthalocyanine derivatives. In general, discotic liquid crystalline phthalocyanines are considered promising organic semiconductors for VOC sensing applications because their sensing performance is governed not only by molecular structure but also by supramolecular organization, particularly the type of mesophase formed. Their ability to self-assemble into columnar architectures provides efficient one-dimensional charge transport pathways, thereby enhancing both electronic communication and analyte interactions [21,86]. Among these mesophases, the columnar hexagonal ($Col_h$) phase offers the most favorable framework for VOC sensing due to its highly ordered arrangement and hexagonal symmetry. This organization strengthens π–π stacking interactions and generates well-defined diffusion channels that facilitate analyte penetration and adsorption. As a result, adsorption-induced modulation of the electronic properties may become more pronounced, potentially leading to enhanced sensor sensitivity and response behavior [87]. The variations in sensing performance can be attributed to the different liquid crystalline organizations of the two phthalocyanine derivatives, which influence molecular packing, analyte diffusion pathways, and charge transport processes

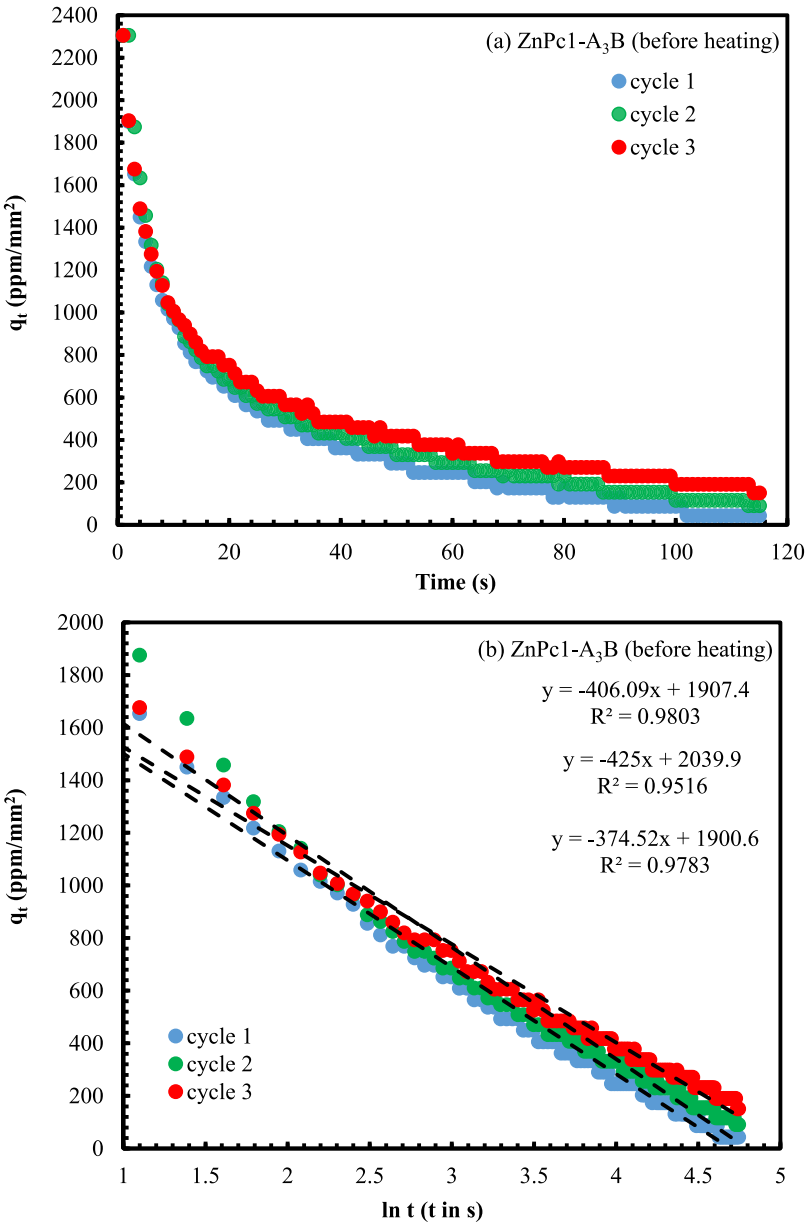


**Fig. 12.** Elovich model adsorption graphs for the ZnPc1-$A_3B$ thin film a) $q_t$ versus t, b) $q_t$ versus ln t.

**Table 7**
The Elovich Model results for ZnPc1-$A_3B$ and ZnPc2-$AB_3$ thin films.

| Elovich model parameter | Cycle | ZnPc1-$A_3B$ thin film | | ZnPc2-$AB_3$ thin film | |
|---|---|---|---|---|---|
| | | Before heating | After heating | Before heating | After heating |
| a | 1st | 44.5141 | 39.9012 | 41.5144 | 42.5505 |
| x$10^{-3}$ (ppm/mm$^2$) | 2nd | 51.6297 | 38.9848 | 44.5803 | 42.9603 |
| | 3rt | 59.8985 | 69.1854 | 52.1763 | 45.4750 |
| b | 1st | 2.463 | 2.386 | 2.365 | 2.137 |
| x$10^3$ (mm$^2$s/ppm) | 2nd | 2.353 | 2.829 | 2.533 | 2.247 |
| | 3rt | 2.67 | 2.608 | 2.702 | 2.353 |
| $\bar{a} \pm \sigma$ x$10^{-3}$ (ppm/mm$^2$) | | 52.0141 ±7.69 | 49.3571 ±17.17 | 46.0903 ±5.48 | 43.6619 ±1.58 |
| $\bar{b} \pm \sigma$ x$10^3$ (mm$^2$s/ppm) | | 2.495 ±0.16 | 2.607 ±0.221 | 2.533 ±0.168 | 2.245 ±0.108 |

within the columnar structures.

## 4. Conclusion

In this study, novel asymmetric zinc(II) phthalocyanines bearing peripheral alkylthio and (dioxyethylene)oxy substituents were successfully synthesized and structurally elucidated by conventional spectroscopic methods, while their liquid crystalline behaviors were systematically investigated through mesophase transition analyses. The ZnPc1-$A_3B$ thin film sensor against DCM vapor yielded the highest sensitivity with the lowest LOD and LOQ values before and after heating processes compared with the ZnPc1-A3B and ZnPc2-$B_4$ thin film sensors. The polyoxoethylene side chains having oxygen atoms improve sensor performance parameters. The ZnPc1-$A_3B$ material could be a good candidate for the detection of DCM vapor at room temperature sensor applications.

Considering the liquid crystalline properties, it is observed that the two phthalocyanine derivatives exhibit different mesophases. While ZnPc1-$A_3B$ displays a columnar rectangular ($Col_r$) phase, ZnPc2-$AB_3$ exhibits a columnar hexagonal ($Col_h$) mesophase. This difference in liquid crystalline behavior, which arises from variations in their

chemical structures, also influences the sensing properties of these compounds toward DCM. It is well known that the sensor response in liquid crystal materials is primarily dependent on the interactions between the analyte and LC molecules, as confirmed by this study. In addition, this work elucidates the role of phthalocyanine molecular architecture and the controlled incorporation of polyoxyethylene and alkylthio substituents in governing charge-transport modulation, thereby determining the sensitivity towards DCM vapor.

## Author statement

All co-authors have viewed the manuscript and agree with the work described. There is no conflict of interest and permission has been granted by the funding body for the work to be submitted for publication and the work is not currently under review elsewhere and shall not be published elsewhere if accepted by this journal.

## CRediT authorship contribution statement

**Zeynep Özer:** Writing – review & editing, Visualization, Validation, Investigation, Formal analysis, Data curation, Conceptualization. **Gizem Gümüşgöz Çelik:** Writing – review & editing, Visualization, Validation, Investigation, Formal analysis, Data curation, Conceptualization. **İnci Çapan:** Writing – review & editing, Visualization, Validation, Methodology, Investigation, Formal analysis, Data curation, Conceptualization. **Rifat Çapan:** Writing – review & editing, Visualization, Validation, Supervision, Methodology, Investigation, Formal analysis, Data curation, Conceptualization. **Ayşe Gül Gürek:** Writing – review & editing, Visualization, Validation, Supervision, Project administration, Methodology, Investigation, Funding acquisition, Formal analysis, Data curation, Conceptualization.

## Declaration of competing interest

The authors declare that they have no known competing financial interests or personal relationships that could have appeared to influence the work reported in this paper.

## Acknowledgements

ZÖ and AGG gratefully acknowledge the Scientific and Technological Research Council of Türkiye (TÜBİTAK) for financial support through the 2209-A Research Project Support Programme for Undergraduate Students (Project No.1919B012304747).

## Supplementary materials

Supplementary material associated with this article can be found, in the online version, at doi:10.1016/j.surfin.2026.109958.

## Data availability

Data will be made available on request.

## References

[1] N.B. McKeown, Phthalocyanine Materials: Synthesis, Structure, Function, Cambridge Univ. Press, Cambridge, 1998, pp. 25–89.
[2] S.Z. Topal, Ü. İşci, U. Kumru, D. Atilla, A.G. Gürek, C. Hirel, M. Durmuş, J.-B. Tommasino, D. Luneau, S. Berber, F. Dumoulin, V. Ahsen, Modulation of the electronic and spectroscopic properties of Zn(ii) phthalocyanines by their substitution pattern, Dalton. Trans. 43 (2014) 6897, https://doi.org/10.1039/c3dt53410c.
[3] A.G. Martynov, J. Mack, A.K. May, T. Nyokong, Y.G. Gorbunova, A.Y. Tsivadze, Methodological survey of simplified TD-DFT methods for fast and accurate interpretation of UV–Vis–NIR spectra of phthalocyanines, ACS Omega 4 (2019) 7265–7284, https://doi.org/10.1021/acsomega.8b03500.
[4] M.C. Vebber, N.A. Rice, J.L. Brusso, B.H. Lessard, Thermodynamic property–performance relationships in silicon phthalocyanine-based organic photovoltaics, ACS Appl. Energy Mater. 5 (2022) 3426–3435, https://doi.org/10.1021/acsaem.1c04013.
[5] Y. Zhang, J.F. Lovell, Recent applications of phthalocyanines and naphthalocyanines for imaging and therapy, WIREs Nanomed. Nanobiotechnol. 9 (2017), https://doi.org/10.1002/wnan.1420.
[6] V. Almeida-Marrero, E. van de Winckel, E. Anaya-Plaza, T. Torres, A. de la Escosura, Porphyrinoid biohybrid materials as an emerging toolbox for biomedical light management, Chem. Soc. Rev. 47 (2018) 7369–7400, https://doi.org/10.1039/c7cs00554g.
[7] P.-C. Lo, M.S. Rodríguez-Morgade, R.K. Pandey, D.K.P. Ng, T. Torres, F. Dumoulin, The unique features and promises of phthalocyanines as advanced photosensitisers for photodynamic therapy of cancer, Chem. Soc. Rev. 49 (2020) 1041–1056, https://doi.org/10.1039/c9cs00129h.
[8] D. Gounden, N. Nombona, W.E. van Zyl, Recent advances in phthalocyanines for chemical sensor, non-linear optics (NLO) and energy storage applications, Coor. Chem. Rev. 420 (2020) 213359, https://doi.org/10.1016/j.ccr.2020.213359.
[9] A.I. Ruiz-Carmuega, C. Garcia-Hernandez, J. Ortiz, C. Garcia-Cabezon, F. Martin-Pedrosa, Á. Sastre-Santos, M.A. Rodríguez-Perez, M.L. Rodriguez-Mendez, Electrochemical sensors modified with combinations of sulfur containing phthalocyanines and capped gold nanoparticles: a study of the influence of the nature of the interaction between sensing materials, Nanomaterials 9 (2019) 1506, https://doi.org/10.3390/nano9111506.
[10] E. Genc, A.C. Yüzer, G. Yanalak, E. Harputlu, E. Aslan, K. Ocakoglu, M. Ince, I. H. Patir, The effect of central metal in phthalocyanine for photocatalytic hydrogen evolution via artificial photosynthesis, Renew. Energy 162 (2020) 1340–1346, https://doi.org/10.1016/j.renene.2020.08.063.
[11] M. Urbani, M.-E. Ragoussi, M.K. Nazeeruddin, T. Torres, Phthalocyanines for dye-sensitized solar cells, Coor, Chem. Rev. 381 (2019) 1–64, https://doi.org/10.1016/j.ccr.2018.10.007.
[12] S. Mai, W. Zhang, X. Mu, J. Cao, Structural decoration of porphyrin/phthalocyanine photovoltaic materials, ChemSusChem. 17 (2024), https://doi.org/10.1002/cssc.202400217.
[13] G. Gümüşgöz Çelik, A.N. Şahin, F. Lafzi, N. Saracoglu, A. Altındal, A.G. Gürek, D. Atilla, Triphenylamine substituted copper and zinc phthalocyanines as alternative hole-transporting materials for solution-processed perovskite solar cells, Dalton. Trans. 51 (2022) 9385–9396, https://doi.org/10.1039/d2dt00068g.
[14] H. Peisert, J. Uihlein, F. Petraki, T. Chassé, Charge transfer between transition metal phthalocyanines and metal substrates: the role of the transition metal, J. Electron. Spec. Relat. Phenom. 204 (2015) 49–60, https://doi.org/10.1016/j.elspec.2015.01.005.
[15] S. Bednarik, J. Demuth, J. Kernal, M. Miletin, P. Zimcik, V. Novakova, Tuning electron-accepting properties of phthalocyanines for charge transfer processes, Inorg. Chem. 63 (2024) 8799–8806, https://doi.org/10.1021/acs.inorgchem.4c00527.
[16] N. Kobayashi, H. Ogata, N. Nonaka, E.A. Luk'yanets, Effect of peripheral substitution on the electronic absorption and fluorescence spectra of metal-free and zinc phthalocyanines, Chem. Eur. J. 9 (2003) 5123–5134, https://doi.org/10.1002/chem.200304834.
[17] T. Nyokong, Effects of substituents on the photochemical and photophysical properties of main group metal phthalocyanines, coor, Chem. Rev. 251 (2007) 1707–1722, https://doi.org/10.1016/j.ccr.2006.11.011, 251.
[18] Y. Sivalingam, G. Magna, R. Kalidoss, S. Murugan, D. Chidambaram, V. Nutalapati, S.V. Jayaraman, R. Paolesse, C. Di Natale, Combinatorial selectivity with an array of phthalocyanines functionalized TiO 2 /ZnO heterojunction thin film sensors, Nanotechnology 33 (2022) 075503, https://doi.org/10.1088/1361-6528/ac378a.
[19] M.K. Rana, M. Sinha, S. Panda, Gas sensing behavior of metal-phthalocyanines: effects of electronic structure on sensitivity, Chem. Phys. 513 (2018) 23–34, https://doi.org/10.1016/j.chemphys.2018.06.021.
[20] T. Basova, A. Hassan, M. Durmuſ, A.G. Gürek, V. Ahsen, Liquid crystalline metal phthalocyanines: structural organization on the substrate surface, Coord. Chem. Rev. 310 (2016) 131–153, https://doi.org/10.1016/j.ccr.2015.11.005.
[21] S. Sergeyev, W. Pisula, Y.H. Geerts, Discotic liquid crystals: a new generation of organic semiconductors, Chem. Soc. Rev. 36 (2007) 1902, https://doi.org/10.1039/b417320c.
[22] T.V. Basova, D.V. Belykh, A.S. Vashurin, D.D. Klyamer, O.I. Koifman, P.O. Krasnov, T.N. Lomova, I.V. Loukhina, E.V. Motorina, G.L. Pakhomov, M.S. Polyakov, A. S. Semeikin, P.A. Stuzhin, A.S. Sukhikh, V.V. Travkin, Tetrapyrrole macroheterocyclic compounds, structure–property relationships, J. Struct. Chem. 64 (2023) 766–852, https://doi.org/10.1134/s0022476623050037.
[23] V. Ivanova, T. Basova, D. Klyamer, A. Sukhikh, S.I. Büyükekşi, D. Atilla, A. G. Gürek, Effect of the number and position of substituents on the orientation and sensor response of triethylene glycol-substituted silicon phthalocyanine films to ammonia, New. J. Chem. 49 (2025) 8279–8288, https://doi.org/10.1039/d5nj00507h.
[24] E.N. Kaya, S. Tuncel, T.V. Basova, H. Banimuslem, A. Hassan, A.G. Gürek, V. Ahsen, M. Durmuş, Effect of pyrene substitution on the formation and sensor properties of phthalocyanine-single walled carbon nanotube hybrids, Sens. Actuators B: Chem. 199 (2014) 277–283, https://doi.org/10.1016/j.snb.2014.03.101.
[25] S. Tuncel, E.N. Kaya, M. Durmuş, T. Basova, A.G. Gürek, V. Ahsen, H. Banimuslem, A. Hassan, Distribution of single-walled carbon nanotubes in pyrene containing liquid crystalline asymmetric zinc phthalocyanine matrix, Dalton. Trans. 43 (2014) 4689, https://doi.org/10.1039/c3dt52736k.
[26] E.N. Kaya, M.S. Polyakov, T.V. Basova, M. Durmuş, A. Hassan, Pyrene containing liquid crystalline asymmetric phthalocyanines and their composite materials with

single-walled carbon nanotubes, J. Porphyr. Phthalocyanines. 22 (2018) 56–63, https://doi.org/10.1142/s1088424618500025.
[27] F. Kus, C. Tasaltin, M. Albakour, A.G. Gürek, İ. Gürol, Macromolecular hexa-asymmetric zinc(II) phthalocyanines bearing triazole-modified triphenylene core: synthesis, spectroscopy and analysis towards volatile organic compounds on surface acoustic wave devices, J. Porphyr. Phthalocyanines. 23 (2019) 477–488, https://doi.org/10.1142/s1088424619500342.
[28] X. Ding, H. Zhu, H. Xu, D. Jiang, The influence of heat-pretreatment on the gas-sensing properties of novel zinc phthalocyanine LB films, J. Porphyr. Phthalocyanines. 06 (2002) 366–370, https://doi.org/10.1142/S1088424602000440.
[29] B. Köksoy, D. Akyüz, A. Şenocak, Mahmut Durmus¸ Erhan Demirbas, Novel SWCNT-hybrid nanomaterial functionalized with subphthalocyanine substituted asymmetrical zinc (II) phthalocyanine conjugate: design, synthesis, characterization and sensor properties for pesticides, Sens. Actuators: B Chem. 329 (2021) 129198, https://doi.org/10.1016/j.snb.2020.129198.
[30] M. Pamukçu Polat, D. Akyüz, H.Y. Yenilmez, A. Koca, Ahmet Altındal Zehra Altuntaş Bayır, sensing alcohol vapours with novel unsymmetrically substituted metallophthalocyanines, Dalton. Trans. 48 (2019) 9194–9204, https://doi.org/10.1039/c9dt01409h.
[31] E.N Kaya, T. Basova, M. Polyakov, M. Durmus, B. Kadem, A. Hassand, Hybrid materials of pyrene substituted phthalocyanines with single-walled carbon nanotubes: structure and sensing properties, RSC Adv. 5 (2015) 91855–91862, https://doi.org/10.1039/c5ra18697h.
[32] N. Esra, M.S. Kayaa, T.V. Polyakovb, Basova*b,c, Mahmut Durmus¸a and Aseel Hassand Pyrene containing liquid crystalline asymmetric phthalocyanines and their composite materials with single-walled carbon nanotubes J, Porphyr. Phthalocyanines 22 (2018) 56–63, https://doi.org/10.1142/S1088424618500025.
[33] M.H. Jodaylami, J.-F. Masson, A. Badia, Surface plasmon resonance sensing, Nat. Rev. Methods Primers. 5 (2025), https://doi.org/10.1038/s43586-025-00417-8.
[34] T. Basova, Phthalocyanine and porphyrin derivatives and their hybrid materials in optical sensors based on the phenomenon of surface plasmon resonance, Chemosensors 12 (2024) 56, https://doi.org/10.3390/chemosensors12040056.
[35] G. Settimo, Y. Yu, M. Gola, M. Buffoli, S. Capolongo, Challenges in IAQ for indoor spaces: a comparison of the reference guideline values of indoor air pollutants from the governments and international institutions, Atmosphere 14 (2023) 633, https://doi.org/10.3390/atmos14040633.
[36] N. Yang, Dichloromethane, in: P. Wexler (Ed.), In Encyclopedia of Toxicology, 3rd ed., Academic Press, Cambridge, MA, USA, 2014, pp. 99–101, https://doi.org/10.1016/b978-0-12-386454-3.01218-5.
[37] Z. Özer, G. Gümüşgöz Çelik, I. Capan, B. Dedeoglu, A.G. Gürek, R. Çapan, Heating effect on the liquid-crystalline octakis(hexylthio)zinc(ii) phthalocyanine thin film sensor for the detection of chlorinated hydrocarbon vapors and interaction mechanism analysis using density functional theory, ACS Omega 11 (2026) 2034–2045, https://doi.org/10.1021/acsomega.5c10679.
[38] V. Ivanova, D. Klyamer, P. Krasnov, E.N. Kaya, I. Kulu, S. Tuncel Kostakoğlu, M. Durmuş, T. Basova, Hybrid materials based on pyrene-substituted metallo phthalocyanines as sensing layers for ammonia detection: effect of the number of pyrene substituents, Sens. Actuators B: Chem. 375 (2023) 132843, https://doi.org/10.1016/j.snb.2022.132843.
[39] Y. Acikbas, M. Erdogan, R. Capan, C. Ozkaya, Y. Baygu, N. Kabay, Y. Gök, Preparation of Zinc (II) phthalocyanine-based LB thin film: experimental characterization, the determination of some optical properties and the investigation of the optical sensing ability, Optik 245 (2021) 167661, https://doi.org/10.1016/j.ijleo.2021.167661.
[40] V. Ivanova, D. Klyamer, G. Tunç, F.D. Gürbüz, D. Atilla, A.G. Gürek, A. Sukhikh, T. Basova, Films of substituted zinc phthalocyanines as active layers of chemiresistive sensors for ammonia detection, New. J. Chem. 47 (2023) 19633–19645, https://doi.org/10.1039/d3nj03400c.
[41] E.N. Kaya, A. Şenocak, D.D. Klyamer, E. Demirbaş, T.V. Basova, M. Durmuş, Ammonia sensing performance of thin films of cobalt(II) phthalocyanine bearing fluorinated substituents, J. Mater. Sci.: Mater. Electron. 30 (2019) 7543–7551, https://doi.org/10.1007/s10854-019-01068-8.
[42] Y. Acikbas, M. Erdogan, R. Capan, C. Ozkaya Erdogan, Y. Baygu, N. Kabay, Y. Gök, G. Kucukyildiz, Preparation and characterization of the phthalocyanine–zinc(II) complex-based nanothin films: optical and gas-sensing properties, Appl. Nanosci. 13 (2023) 4527–4540, https://doi.org/10.1007/s13204-022-02749-3.
[43] Y. Çimen, E. Ermiş, F. Dumludağ, A.R. Özkaya, B. Salih, Ö. Bekaroğlu, Synthesis, characterization, electrochemistry and VOC sensing properties of novel ball-type dinuclear metallophthalocyanines, Sens. Actuators B: Chem. 202 (2014) 1137–1147, https://doi.org/10.1016/j.snb.2014.06.066.
[44] T. Ceyhan, A. Altındal, M.K. Erbil, Ö. Bekaroğlu, Synthesis, characterization, conduction and gas sensing properties of novel multinuclear metallo phthalocyanines (Zn, Co) with alkylthio substituents, Polyhedron 25 (2006) 737–746, https://doi.org/10.1016/j.poly.2005.07.046.
[45] J. Spadavecchia, G. Ciccarella, P. Siciliano, S. Capone, R. Rella, Spin-coated thin films of metal porphyrin–phthalocyanine blend for an optochemical sensor of alcohol vapours, Sens. Actuators B: Chem. 100 (2004) 88–93, https://doi.org/10.1016/j.snb.2003.12.027.
[46] N.E. Duran, İ. Çapan, Macrocycle ring and peripheral group sizes-dependent vapor sensing property of copper phthalocyanine thin films, Surf. Rev. Lett. 27 (2020) 2050006, https://doi.org/10.1142/s0218625x20500067.
[47] T. Basova, E. Kol'tsov, A.K. Ray, A.K. Hassan, A.G. Gürek, V. Ahsen, Liquid crystalline phthalocyanine spun films for organic vapour sensing, Sens. Actuators B: Chem. 113 (2006) 127–134, https://doi.org/10.1016/j.snb.2005.02.038.
[48] R. Capan, I. Capan, F. Davis, A new approach for the adsorption kinetics using surface plasmon resonance results, Sens. Actuators B: Chem. 394 (2023) 134463, https://doi.org/10.1016/j.snb.2023.134463.
[49] Ş. Altın, F. Dumludag, Ç. Oruç, A. Altındal, Influence of humidity on kinetics of xylene adsorption onto ball-type hexanuclear metallophthalocyanine thin film, Microelectron. Eng. 134 (2015) 7–13, https://doi.org/10.1016/j.mee.2015.01.009.
[50] F.C. Wua, R.L. Tseng, R.S. Juang, Characteristics of Elovich equation used for the analysis of adsorption kinetics in dye-chitosan systems, Chem. Eng. J. 150 (2009) 366–373, https://doi.org/10.1016/j.cej.2009.01.014.
[51] M. Pişkin, N. Can, Z. Odabas, A. Altındal, Toluene vapor sensing characteristics of novel copper(II), indium(III), mono-lutetium(III) and tin(IV) phthalocyanines substituted with 2,6-dimethoxyphenoxy bioactive moieties, J. Porphyr. Phthalocyanines. 22 (2018) 189–197, https://doi.org/10.1142/S1088424617500900.
[52] A.G. Gürek, Ö. Bekaroğlu, Octakis(alkylthio)-substituted phthalocyanines and their interactions with silver(I) and palladium-(II) ions, J. Chem. Soc. Dalton Trans. 9 (1994) 1419–1423, https://doi.org/10.1039/DT9940001419.
[53] N.B. McKeown, I. Chambrier, M.J. Cook, Synthesis and characterisation of some 1,4,8,11,15,18,22,25-octa-alkyl- and 1,4,8,11,15,18-hexa-alkyl-22,25-bis (carboxypropyl)phthalocyanines, J. Chem. Soc. Perkin Trans. 1 (1990) 1169, https://doi.org/10.1039/p19900001169.
[54] R. Jung, M. Hanack, Preparation and Diels-Alder reactions of new nickel phthalocyanines, Synt. Met. 102 (1999) 1526, https://doi.org/10.1016/s0379-6779(98)90016-9.
[55] S.V. Kudrevich, H. Ali, J.E. van Lier, Syntheses of monosulfonated phthalocyanines, benzonaphthoporphyrazines and porphyrins via the Meerwein reaction, J. Chem. Soc. Perkin Trans. 1 (1994) 2767, https://doi.org/10.1039/p19940002767.
[56] T.G. Linssen, K. Dürr, M. Hanack, A. Hirsch, A green fullerene: synthesis and electrochemistry of a Diels–Alder adduct of [60]fullerene with a phthalocyanine, J. Chem. Soc. Chem. Commun. (1995) 103–104, https://doi.org/10.1039/c39950000103.
[57] E.M. Maya, C. García, E.M. García-Frutos, P. Vázquez, T. Torres, Synthesis of novel push−pull unsymmetrically substituted alkynyl phthalocyanines, J. Org. Chem. 65 (2000) 2733–2739, https://doi.org/10.1021/jo991843f.
[58] S. Makhseed, A. Cook, N.B. McKeown, Phthalocyanine-containing polystyrenes, Chem. Commun. (1999) 419–420, https://doi.org/10.1039/a900069k.
[59] G. de la Torre, C.G. Claessens, T. Torres, Phthalocyanines: the need for selective synthetic approaches, Eur. J. Org. Chem. (2000) 2821–2830, https://doi.org/10.1002/1099-0690(200008)2000, 200016≤2821::aid-ejoc2821≥3.0.co;2-2.
[60] D. Atilla, N. Saydan, M. Durmuş, A.G. Gürek, T. Khan, A. Rück, H. Walt, T. Nyokong, V. Ahsen, Synthesis and photodynamic potential of tetra- and octa-triethyleneoxysulfonyl substituted zinc phthalocyanines, J. Photochem. Photobiol. A: Chem. 186 (2007) 298–307, https://doi.org/10.1016/j.jphotochem.2006.08.022.
[61] E.T. Saka, M. Durmuş, H. Kantekin, Solvent and central metal effects on the photophysical and photochemical properties of 4-benzyloxybenzoxy substituted phthalocyanines, J. Organomet. Chem. 696 (2011) 913–924, https://doi.org/10.1016/j.jorganchem.2010.10.024.
[62] L. Kaestner, M. Cesson, K. Kassab, T. Christensen, P.D. Edminson, M.J. Cook, I. Chambrier, G. Jori, Zinc octa-n-alkyl phthalocyanines in photodynamic therapy: photophysical properties, accumulation and apoptosis in cell cultures, studies in erythrocytes and topical application to balb/c mice skin, Photochem. Photobiol. Sci. 2 (2003) 660–667, https://doi.org/10.1039/b211348a.
[63] J. Tant, Y.H. Geerts, M. Lehmann, V. De Cupere, G. Zucchi, B.W. Laursen, T. Bjørnholm, V. Lemaur, V. Marcq, A. Burquel, E. Hennebicq, F. Gardebien, P. Viville, D. Beljonne, R. Lazzaroni, J. Cornil, Liquid crystalline metal-free phthalocyanines designed for charge and exciton transport, J. Phys. Chem. B 110 (2006) 3449, https://doi.org/10.1021/jp060109e. -34493449–3449.
[64] T.V. Basova, M. Çamur, A.A. Esenpınar, S. Tuncel, A. Hassan, A. Alexeyev, H. Banimuslem, M. Durmuş, A.G. Gürek, V. Ahsen, Effect of substituents on the orientation of octasubstituted copper(II) phthalocyanine thin films, Synt. Met. 162 (2012) 735–742, https://doi.org/10.1016/j.synthmet.2012.02.006.
[65] A.G. Gürek, V. Ahsen, F. Heinemann, P. Zugenmaier, Synthesis and liquid-crystalline behaviour of tetrakis- and octakis(13, 17-dioxa nonacosane-15-sulfanyl) phthalocyanines, molecular crystals and liquid crystals science and technology, A Mol. Cryst. Liq. Cryst. 338 (2000) 75–97, https://doi.org/10.1080/10587250008024421.
[66] T.V. Basova, A.G. Gürek, V. Ahsen, Investigation of liquid-crystalline behavior of nickel octakisalkylthiophthalocyanines and orientation of their films, Mat. Sci. Eng. C 22 (2002) 99–104, https://doi.org/10.1016/s0928-4931(02)00051-6.
[67] S. Dabak, V. Ahsen, F. Heinemann, P. Zugenmaier, Synthesis and characterization of novel tetra- and octa-triethyleneoxysulfanyl substituted phthalocyanines forming lyotropic mesophases, molecular crystals and liquid crystals science and technology, Mol. Cryst. Liq. Cryst. 348 (2000) 111–127, https://doi.org/10.1080/10587250008024800.
[68] D. Atilla, G. Aslıbay, A.G. Gürek, H. Can, V. Ahsen, Synthesis and characterization of liquid crystalline tetra- and octa-substituted novel phthalocyanines, Polyhedron 26 (2007) 1061–1069, https://doi.org/10.1016/j.poly.2006.09.105.
[69] R. Çapan, H. Göktaş, Z. Özbek, S. Şen, M.E. Özel, F. Davis, Langmuir–Blodgett thin film for chloroform detection, Appl. Surf. Sci. 350 (2015) 129–134, https://doi.org/10.1016/j.apsusc.2015.02.109.
[70] K. Vazirinezhad, F. Shariatmadar Tehrani, S. Zeinali, M. Tohidi, Fabrication of highly efficient quartz crystal microbalance ammonia sensor based on Cu-BTC

nanocomposites, J. Sci.: Adv. Mater. Dev. 10 (2025) 100850, https://doi.org/10.1016/j.jsamd.2025.100850.
[71] S.D. Lawaniya, S. Kumar, Y. Yu, H.-G. Rubahn, Y.K. Mishra, K. Awasthi, Functional nanomaterials in flexible gas sensors: recent progress and future prospects, Mat. Today Chem. 29 (2023) 101428, https://doi.org/10.1016/j.mtchem.2023.101428.
[72] E. Haghighi, S. Zeinali, Formaldehyde detection using quartz crystal microbalance (QCM) nanosensor coated by nanoporous MIL-101(Cr) film, microporous and mesoporous mat. 300 (2020) 110065. https://doi.org/10.1016/j.micromeso.2020.110065.
[73] Y.M. Rohman, R. Sukowati, A. Priyanto, D.A. Hapidin, D. Edikresnha, K. Khairurrijal, Quartz crystal microbalance coated with Polyacrylonitrile/nickel nanofibers for high-performance methanol gas detection, ACS Omega 8 (2023) 13342–13351, https://doi.org/10.1021/acsomega.3c00760.
[74] R. Capan, I. Capan, M. Bayrakci, Rhodamine-based electrospun polyacrylonitrile (pan) nanofiber sensor for the detection of chlorinated hydrocarbon vapors, ACS Appl. Polym. Mater. 6 (2024) 7500–7511, https://doi.org/10.1021/acsapm.4c00909.
[75] L. Katriani, R. Aflaha, C.N. Maharani, F. Naafi'ah Salsabila, A.H. As'ari, A. Rianjanu, P. Nurwantoro, R. Roto, K. Triyana, Quartz Crystal microbalance coated with a polyvinylpyrrolidone microfiber active layer as a high-performance acetic acid gas sensor, Langmuir 41 (2025) 4632–4640, https://doi.org/10.1021/acs.langmuir.4c04474.
[76] R. Roto, A. Rianjanu, A. Rahmawati, I.A. Fatyadi, N. Yulianto, N. Majid, I. Syamsu, H.S. Wasisto, K. Triyana, Quartz crystal microbalances functionalized with citric acid-doped polyvinyl acetate nanofibers for ammonia sensing, ACS Appl. Nano Mater. 3 (2020) 5687–5697, https://doi.org/10.1021/acsanm.0c00896.
[77] A.N. Kursunlu, Y. Acikbas, C. Yilmaz, M. Ozmen, I. Capan, R. Capan, K. Buyukkabasakal, A. Senocak, Sensing volatile pollutants with spin-coated films made of pillar[5]arene derivatives and data validation via artificial neural networks, ACS Appl. Mater. Interfaces. 16 (2024) 31851–31863, https://doi.org/10.1021/acsami.4c06970.
[78] I. Capan, A.N. Kursunlu, Y. Acikbas, E. Yemisci, R. Capan, M. Ozmen, Novel pillar[6]arene thin films for enhanced gas sensing of volatile organic compounds, J. Mol. Struct. 1355 (2026) 145031, https://doi.org/10.1016/j.molstruc.2025.145031.
[79] S. Şen, Z. Özbek, F. Aydin, R. Capan, Investigation of gas sensing properties of organic π–π* complexes spin coated thin films in dry and humid environment, J. Mater. Sci.: Mater. Electron. 36 (2025), https://doi.org/10.1007/s10854-025-16282-w.
[80] R. Çapan, İ. Çapan, F. Davis, A.K. Ray, Spin-coated films of calix[4]resorcinarenes as sensors for chlorinated solvent vapours, J. Mater. Sci.: Mater. Electron. 35 (2024), https://doi.org/10.1007/s10854-024-13457-9.
[81] R. Capan, M. Erdogan, I. Capan, C. Ozkaya Erdogan, F.G. Moscoso, J.M. Pedrosa, L. K. Komodiki, A.J. Tasiopoulos, Characterization of Spun PMMA/UiO-66-NH2@PMMA Thin films and their SPR sensing response to haloalkane vapors, IEEE Sens. J. 22 (2022) 18287–18294, https://doi.org/10.1109/jsen.2022.3197497.
[82] A. Hierlemann, A.J. Ricco, K. Bodenhöfer, W. Göpel, Effective use of molecular recognition in gas sensing: results from acoustic wave and in situ FT-IR measurements, Anal. Chem. 71 (1999) 3022–3035, https://doi.org/10.1021/ac981311j.
[83] L.H. Huo, X.L. Li, W. Li, S.Q. Xi, Gas sensitivity of composite Langmuir-Blodgett films of Fe2O3 nanoparticle-copper phthalocyanine, Sens. Actuators B: Chem. 71 (2000) 77–81, https://doi.org/10.1016/s0925-4005(00)00605-5.
[84] T.V. Basova, C. Tasaltin, A.G. Gürek, M.A. Ebeoğlu, Z.Z. Öztürk, V. Ahsen, Mesomorphic phthalocyanine as chemically sensitive coatings for chemical sensors, Sens. Actuators B: Chem. 96 (2003) 70–75, https://doi.org/10.1016/S0925-4005(03)00487-8.
[85] S. Harbeck, S. Göçmen, Ö.F. Emirik, Z.Z. Öztürk, V. Ahsen, A.G. Gürek, Synthesis of branched alkoxy side chains containing phthalocyaninederivates and their application in mass sensitive QCM sensors, Sens. Actuators B: Chem. 233 (2016) 55–62. http://doi.org/10.1016/j.snb.2016.04.038.
[86] I.W.T. Wöhrle, J. Kirres, A. Kostidou, N. Kapernaum, J. Litterscheidt, J.C. Haenle, P. Staffeld, A. Baro, F. Giesselmann, S. Laschat, Discotic liquid crystals, Chem. Rev. 116 (2016) 1139–1241, https://doi.org/10.1021/acs.chemrev.5b00190.
[87] F.I. Bohrer, A. Sharoni, C. Colesniuc, J. Park, I.K. Schuller, A.C. Kummel, W. C. Trogler, Gas sensing mechanism in chemiresistive cobalt and metal-free phthalocyanine thin films, J. Am. Chem. Soc. 129 (2007) 5640–5646, https://doi.org/10.1021/ja0689379, 129.